Complex patterns of neuronal activity underpin a global change in brain state during walk in *Drosophila*

Sophie Aimon[1#], Karen Y. Cheng[1], Julijana Gjorgjieva[1,2] and Ilona C. Grunwald Kadow[1,3]

1 Technical University of Munich, School of Life Sciences, 85354 Freising, Germany
2 Max Planck Institute for Brain Research, Computation in Neural Circuits, 60438 Frankfurt, Germany
3 University of Bonn, Medical Faculty, Institute of Physiology II, 53115 Bonn, Germany
new address: Max Planck Institute for Biological Cybernetics, 72076 Tübingen, Germany

Corresponding authors: Sophie Aimon, sophie.aimon@gmail.com
Ilona C. Grunwald Kadow, ilona.grunwald@uni-bonn.de

Abstract

Movement influences sensory perception and behavior. Here, we used fast wholebrain lightfield imaging in adult *Drosophila* to analyze the relationship between walk and neuronal activity. We observed brainwide activity that tightly correlated with spontaneous bouts of walk. While imaging of specific sets of excitatory, inhibitory, and neuromodulatory neurons highlighted their joint contribution, different subsets displayed distinct spatial distribution and dynamics before, during, and after walk onset. Using computational tools, we mapped forward walk- and turning-induced activity onto different brain subregions and sometimes individual neurons, and thereby identified regions not previously implicated in walk. In particular, a subset of serotonergic neurons in the lateral protocerebrum stood out for being inhibited during walk. Finally, we found that spontaneous and forced forward walk elicited highly similar global activity, suggesting a major contribution of walk and walk-related sensory or proprioceptive information to brain state. We concluded that walk-related signals induce global but heterogeneous patterns of activity, allowing for differential local and brainwide integration of behavioral state into other processes in the brain.

Introduction

Growing evidence from nematodes to mammals shows that ongoing behavior affects brain activity globally [1]. Using a combination of imaging and neuropixel recordings in awake, behaving mice, recent work showed that multiple dimensions of (spontaneous) behavior, including facial or body movements, are represented brainwide, allowing the integration of external or internal stimuli with the current behavioral state [2]. Brainwide imaging at single cell-resolution of calcium activity in *C. elegans* and larval zebrafish indicated that as in mammals, multiple aspects of behavior and motor activity are represented across the brain including areas thought to be dedicated to primary sensory information processing [3]. Importantly, such brainwide representations of motor states are seen independent of visual or olfactory inputs.

Previous studies suggested a similar situation in insects. For example, in *Drosophila melanogaster*, active flight modulates visual motion processing [4]. Similarly, visual horizontal system cells encode quantitative information about the fly's walking behavior independently of visual input [5]. Beyond primary sensory brain areas, several types of dopaminergic neurons innervating the fly's higher brain center, the mushroom body (MB), show activity highly correlated with bouts of walking [6]. Importantly, wholebrain imaging revealed that behavior-related activity occurred in most brain regions and was independent of visual or olfactory input [7]. These and other studies provide convincing evidence for brainwide signatures of behavior across species. However, how behavior-related information is relayed to the brain, how it spreads within neural networks and what it represents remain largely unanswered questions. Complementary to other animal models, the fly provides opportunities to study adult, global brain states associated with behavior at high temporal and spatial resolution due to its small brain size [8]. In addition, recent electron microscopy (EM) connectomics highlighted that neural networks spread across the entire brain with many pathways unrevealed by traditional single neuron manipulation experiments [9]. Adult *Drosophila* behavior has been studied in detail for many years [10], but the resulting or underlying brainwide activity for even just roughly defined behavioral states such as resting or walking remains largely unknown.

Movement in adult *Drosophila* is thought to be controlled by descending neurons connecting the brain to the ventral nerve cord (VNC), which contains local pattern generators [11]. This top-down view is challenged by other studies suggesting that behavioral control is decentralized with feedback loops involving the brain [12], or even that many behaviors could be locally controlled by

neurons in the VNC without involving the brain [e.g., decapitated grooming [13]].

Here, we build on our previous work[8] using fast wholebrain imaging during ongoing behavior to unravel more comprehensively the spatial and temporal relationship between movement and neural network activity across multiple brain structures and neuromodulators. We first identify aspects of the behavior encoded by regions and neurons expressing different neuromodulators. We next characterize the timing of activation at the behavior transitions between rest and walk and find that walk-related activity in most brain regions happens at or after the transition. Nevertheless, higher temporal resolution imaging reveals several activity components, e.g., in the MB, active before walk onset. This is consistent with the hypothesis that brain activity in most regions originates primarily from efferent or proprioceptive feedback, and that few brain regions are directly involved in top-down movement control. We test this hypothesis by comparing global brain activity during forced and spontaneous walk and find them to be highly similar in most brain regions. Our results suggest that walk triggered by activity in select brain areas and neurons elicits a global change in brain state thereby allowing for efficient integration of external information with ongoing behavioral actions to guide appropriate next decisions possibly leading to behavioral adaptation and learning.

Results

Whole brain imaging reveals broad activation during walk

To image wholebrain activity during spontaneous behavior, we fixed the fly's head to a holder and opened the posterior head capsule while leaving the legs free to move [14] (Fig. 1a). As a walkable surface, we used an air-supported ball to assess the fly's walking speed [15](Fig. 1a). We also carried out experiments without a walking substrate to compare activity related to walk to activity related to flailing movements, where the fly moves its legs freely in the air. We expressed GCaMP pan-neuronally (i.e., *nsyb-gal4;UAS-GCaMP6m/f*) and imaged calcium transients as a proxy of neuronal activity in the whole brain using fast lightfield microscopy (LFM) as described previously in detail [8]. Briefly, a multilens array captures an image of the entire brain. This raw image is further processed and corrected for movement artifacts to identify the brain regions or activity components with movement-correlated calcium increases (Fig. 1a). In order to compare periods of rest with periods of spontaneous walk, we combined behavioral movies and z-projections of whole brain data (Video 1). We observed a strong increase in

neuronal activity across the brain during bouts of walking compared to during resting or grooming (Fig. 1b, c).

While LFM allows for very fast imaging frame rates (up to 200 Hz for the whole brain), the frame rate was limited by the signal-to-noise ratio in each individual fly and was thus adjusted for each experiment (see Methods). We found no significant difference between the global activity R^2-values for walk at different frame rates (5 – 98 Hz) for flies expressing GCaMP6f pan-neuronally (Fig. S1a). Thus, we pooled these data for the analysis below regarding global brain state.
In experiments where the fly was both walking and resting, the first principal component (PC1) of the whole brain activity data was strongly correlated to walk (Fig. 1d). Next, by aligning whole brain imaging data to an anatomical template using landmark registration, and by averaging activity in each large anatomically defined region (see Methods), we also found that the global activity of regions correlated with walk (Fig. 1b and c). Importantly, neuronal activation followed movement bouts at high temporal precision (limited by the temporal resolution of the calcium reporter) inconsistent with activity generated by general arousal, which we would not expect to precisely follow such bouts (Fig. 1b and c). However, the calcium responses were still a little slower than some of the fast changes in walking, even after convolution of walking with an impulse response, which suggests that faster calcium probes could capture finer dynamics in further studies (Fig. 1c).

We next mapped the differences in activity during walk, flail, or groom to a brain template with finer brain regions to understand their spatial organization. While we still observed an increase in activity during bouts of flailing, the brain was not as consistently globally activated as during walking (Fig.1e and f). Strikingly, unlike grooming, which resulted in local activation of ventral brain areas consistent with [16], all brain regions were significantly correlated with walking (Fig. 1e and f). Indeed, using walking behavior we were able to explain ~ 20 % of all variances observed in the experiments (R^2 median = 0.194, Fig. 1e). We used a linear model to analyze how the correlation of brain activity with walking (normalized coefficient and the R^2) depended on the brain region. To ensure our results were not biased by heterogeneous expression in the pan-neuronal transgenic driver line, we used two different pan-neuronal lines (*nsyb-Gal4* and *GMR57C10-Gal4*). The linear model (Table 1) showed that there was no significant effect of the Gal4-driver. We found a small but significant effect of the GCaMP version used, however, and thus kept using the model to take this effect into account for the rest of the study. Using this model, we quantified the effect of the distinct brain regions on both the normalized coefficient and the R^2 of the regression with a behavior regressor (Fig. 1g, S1c-g,j,k). While all brain areas

were significantly activated during walk (Fig. 1g, S1c), only the region of the gnathal ganglion (GNG) showed strong activation during grooming (Fig. S1e,g). Flailing represents an intermediate state with many brain regions activated but to a lower degree and less consistently as compared to walk (Fig. 1e, S1d,f). Moreover, the global activity correlated primarily with walk and not with the start or end of walk (Fig. 1h).

To test whether part of the observed global brain activity could be due to visual input coupled with the behavior, e.g., by the fly seeing the optic flow from the ball [17], or unexpectedly fixed reflections from the environment [18], we performed the same experiments but covered the fly's eyes with black nail polish to prevent outside light from activating its photoreceptor neurons. With such strongly limited visual input, we still observed a very similar, not significantly different, global activity pattern indicating that visual input is a minor contributor to the observed wide brain activity (Fig. S1b). This also suggested that the global increase in activity during walk is not due to a mismatch between an actual and a predicted visual stimulus. In addition, given that air-supported balls can show erratic movements due to air turbulences that could cue the fly to change its behavior [19], or impose constraints on the animal's posture, we performed parallel experiments with an unsupported styrofoam ball held by the fly (see Methods). The comparison of the two datasets revealed a significant difference in R^2 for global brain activity (Fig. S1h), indicating that the type of walking substrate influenced brain activation. Given that the activity distribution across brain regions did not significantly differ between the two substrate types at this level of analysis (Fig. S1i), we combined the datasets for most analysis below.

Together these data confirm that walking behavior induces a change in global brain activity[8] with most brain regions showing highly temporally correlated activity during bouts of spontaneous walk. They further suggest that most global activity occurs during walk and not at its start or end. Finally, the data pinpoint brain regions differentially activated during different types of leg movements.

Both inhibitory and excitatory neurons are recruited during walk

To gain more insight into the type of neurons responsible for the global state change of the brain during walk, we expressed GCaMP in different types of neurons and repeated the experiment as described above. For instance, previous work indicated that 37% of all descending neurons (DN) to the ventral nerve cord (VNC) are GABAergic and 38% cholinergic, while 6% express the neurotransmitter glutamate [20].

It is conceivable that broad brain activation arises due to a global disinhibition during periods of walking [21]. To address this possibility, we expressed GCaMP6m exclusively in GABAergic inhibitory neurons using the GAD1-Gal4 driver. We also did the same with a driver for glutamatergic neurons (*Vglut-gal4;UAS-GCaMP6m*) as glutamate is thought to be inhibitory in the fly. In addition, we analyzed activation patterns during behavior in excitatory neurons by imaging from all cholinergic neurons in the fly brain (*Cha-gal4;UAS-GCaMP6m or UAS-GCaMP6f).* Using the same approach and analysis as described above, we detected an increase in global brain activation, which again correlated highly with walking bouts, for excitatory and inhibitory types of neurons (Fig. 2a).

As for the pan-neuronal data, we mapped this activity to all brain regions to create a functional map of activity during walk (Fig. 2b,c). Among other regions, we found that the GNG, the anterior ventral lateral protocerebrum (AVLP) and the antennal mechanosensory and motor center (AMMC), known to be important for leg coordination and to be highly innervated by ascending neurons (AN) from the VNC [22], responded to walk for all genotypes (Fig. 2b-d). Again, brain activity closely followed individual walk bouts (Fig. 2d). Using a linear regression model, we determined that similar to the pan-neuronal data, excitatory neurons labeled by Cha-Gal4 were activated in all brain regions (Fig. 2e, S2a). At a global scale, we observed highly similar activation patterns with neurons labeled by Vglut-Gal4 and GAD-Gal4 being significantly activated during walk (Fig. 2e and S2b,c). Brain regions such as the protocerebral bridge (PB), the cantle (CAN), the vest (VES) and the superior posterior slope (SPS) were correlated especially strongly in all three types of neurons (Fig. S2a-c).

Together these data show that inhibitory neurons as well as excitatory neurons are activated in most brain regions during walk. Moreover, these data suggest that the observed activity in pan-neuronal imaging is not mediated by a global disinhibition in the brain, but rather a result of a combined activation of different types of neurons, including excitatory and inhibitory neurons.

Aminergic neuron activity is strongly correlated with behavior

Monoamine-releasing neuromodulatory neurons, i.e., dopamine, serotonin and octopamine (the fly's equivalent to mammalian noradrenaline) have been shown in the past to be important to control and adjust behavior [23]. However, the role of these neuromodulators during motor behavior remains to be fully elucidated. Among the DNs, these neuromodulatory neurons make up ~4% [20].

Previous data suggested that both walking and flailing, but not grooming or resting, were related to an increase in dopaminergic neuron activity (DAN) [24]. We used different Gal4 drivers for different types of neuromodulatory neurons i.e., Tdc2-Gal4/octopamine and Trh-Gal4/serotonin. For dopamine, we combined TH-Gal4 with DDC-Gal4 or GMR58E04-Gal4 to cover all dopaminergic neuron types [25].

While we observed an increase in activity for all neuromodulatory neuron types[8], serotonergic neurons were significantly less globally activated than dopaminergic and octopaminergic neurons during spontaneous bouts of walk (Fig. 3a and d, Video 2-4). We again also mapped the activity to the regions of the brain (Fig. 3b). Contrary to results shown above with pan-neuronal and broad neurotransmitter lines, maps were distinctly patterned for the individual aminergic lines, as revealed by overlaid activity maps (Fig. 3b,c).

In addition to the MB, most regions were consistently activated by neurons expressing GCaMP6m or GCaMP6f under the control of TH/DDC-Gal4 (Fig. 3b-d, S3a). Importantly, besides the dopaminergic neurons that were already implicated in prior work [26], whole brain imaging suggested that many additional DANs were activated during or due to walk (Fig. 3a-d). Octopaminergic neuron activity (imaged with *Tdc2-gal4;UAS-GCaMP6s*) was also highly correlated with walking (Fig. 3a,b,d). The activation was particularly high for neurons located or projecting into the ventromedial neuropils (VMNP, Fig. 3f and S3b).

Using whole brain imaging of serotonergic neuron activity (*Trh-gal4;UAS-GCaMP6m,f or s*), we found that the activity of several regions was highly correlated with walking (Fig. 3b,e,f). Surprisingly though, the strongest correlation was negative and mapped to the anterior ventrolateral protocerebrum (AVLP) region (Fig. 3b (blue area), 3e,f). This suggested that while some populations of serotonergic neurons were activated, some subsets, in particular in the AVLP, were inhibited during walk (Fig. 3e).

Together, these data show that walking behavior activates, and in some cases inhibits, all main types of aminergic neuromodulatory neurons in various but distinct brain regions. Thus, the observed pan-neuronal global activity during walk is a result of the combined patterns of activation of excitatory, inhibitory, and neuromodulatory neuronal responses to walk.

Wholebrain activity data identifies specific brain regions or even neurons

Global brain activity can be used to generate functional maps of the brain (i.e., fMRI). These functional maps not only show which brain regions are activated but provide information regarding which brain regions might be functionally connected and/or involved in similar aspects

of a task due to their highly correlated activity (i.e., functional connectome). These functional connectomes allow speculations about how information underpinning behavior travels throughout a whole brain. While such data can be generated for other animals including humans, the fly (along with *C. elegans* and in the near future zebrafish) currently provides the important advantage of being able to combine such activity maps with highly detailed anatomical maps from light microscopy with cellular resolution and whole brain EM connectomics with synaptic resolution. Ultimately, such data could be used to generate precise models of how recorded neural activity spreads through a brain. For instance, DNs receive input from regions of the brain that are innervated by outputs from higher brain regions such as the MB and central complex (CC) [20]. DN and AN innervation of the GNG is consistent with an important role of the GNG in motor control and motor feedback integration [27]. How anatomical connectivity relates to activity in widespread neural networks is not clear.

As a first step to study how activities in different brain regions relate to one another, we adjusted the region classification used above to smaller brain regions (from now on referred to as components) or ideally single neuron types [28]. To this end, we extracted functional components using PCA followed by ICA to unmix the PCA maps (see Methods) (Fig. 4a, S4a-c). In essence, ICA unmixes the PCA values in an effort to spatially separate them. We grouped smaller functional components within a larger brain region (e.g., different antennal and protocerebral bridge glomeruli), if the precision of the alignment of the template did not allow a clear assignment of individual regions. Interestingly, almost all functional components derived from recorded neuronal activity matched the above-identified anatomical structures without further subdivisions or blurring of anatomical boundaries. This suggested that the activity within brain regions was more homogenous as compared to the activity in neighboring regions. A few exceptions stood out: for example, our functional data separated a larger region in the lateral neuropil, the AVLP, into smaller subregions (Fig. 4a, S4a,b, orange box) suggesting that subregions of the AVLP had different activity signatures. A similar situation occurred in the MB. Of note, some components also identified more than one brain region (i.e., PENP-SLP) indicating a strong functional, i.e. synaptic, connection between these regions.

Not all components were correlated with walk, thus representing ongoing activity unrelated to walk [29].

Among the components correlating with spontaneous walk, the PENP-SLP (periesophageal neuropils and superior lateral protocerebrum) and PENP-CL (periesophageal neuropils and

clamp) components might contribute to relaying the information that the fly walks from the ventral neuropils (e.g., GNG) to higher areas or vice versa. The WPNb (bilateral wedge projection neuron) component (likely generated by the WPNb neuron [30]) was weakly correlated with walk. Nonetheless, it showed a R^2-value significantly above zero and could thus also relay the activity between higher and lower brain regions.

In addition to the data collected with pan-neuronally expressed GCaMP, we used the same analysis pipeline to assign functional components to the data collected for inhibitory, excitatory and neuromodulatory neurons (Fig. 4a). For dopaminergic neurons, walk-correlated neuronal activity was found, for instance, for components in and around the MB (i.e. γ3-compartment as previously observed; [31], in the central complex (protocerebral bridge (PB) and ellipsoid body (EB), but also in ventral neuropil such as the wedge (WED) and neuropil connecting central regions to the optic lobes (Fig. 4a). For octopamine, one particular component connecting the optic lobe and the periesophageal neuropil was correlated strongly with walk, the OL-PENP, while for serotonin the highest R^2-value was detected for the AVLP and components within (Fig. 4a).

Most components with significant R^2-values were positively correlated with walk with one exception (Fig. 4b,c): a specific component of the AVLP, a subregion we named the AVLPshell due to its shape, was negatively correlated with walk, i.e., was inhibited during walk (Fig. 4b, S4a-c). As this component was mostly detected in the experiment using Trh-Gal4, serotonergic neurons were likely responsible for the decrease in activity during walk (see also Fig. 3).

Several of these components were previously implicated in walking behavior or its modulation, many others were not (Table 2) indicating that whole brain imaging during behavior in combination with our analysis pipeline provides a powerful method to pinpoint new brain regions and neurons involved in the control of, or response to, walking behavior. For most components, we were able to propose specific neurons based on anatomical resemblance (Table 2). Some of these neurons can be labeled by Gal4 transgenic lines for future functional manipulation. Furthermore, the identification of functional components reveals functional similarity and connectivity of anatomically connected brain regions in spontaneous walk.

Turning activates specific brain regions and neurons

Some functional components activated during walk showed an activity that appeared to be

mirrored by the other half of the brain (Fig. 5a). We next asked whether these components had differential activity when turning left or right (Fig. S5). To quantify turning, we extracted rotational ball movement (left and right) using its optic flow and convolved it with the fluorescence increase of GCaMP for each experiment and component. This convolution matched the temporal characteristics of the behavior to brain activity, and smoothed potential jitter from the air supported ball. The speed of the rotational flow, which is proportional to the degree of turning, was on average 0.4 - 2 radian/s. The components that correlated with turning were reproducibly found across different flies based on similar position and morphology (Fig. 5a for examples in *TH/DDC-Gal4;UAS-GcaMP6m*). These included the IPS-Y (inverse Y shape in the posterior slope) and LAL-PS (lateral accessory lobe and posterior slope) as previously mentioned in [8]. We identified candidate neurons for all regions such as DNb02 and DNb01 for IPS-Y and LAL-PS, respectively (Table 2). These DNs were previously described by Namiki et al., who generated specific Gal4 lines for neuronal manipulation [32]. For instance, optogenetic activation of DNb01 induced twitching of the fly's front legs consistent with a role in turning [33]. For dopaminergic neurons, the components most correlated with turning could be matched with specific neurons such as neurons of the PPM2 cluster, i.e., PPM2-LW (PPM2-LAL-WED: PPM2- lateral accessory lobe-wedge [34])(Fig. 5a, right panels; Video 5). By subtracting the coefficient of activity on the contralateral side from the coefficient on the ipsilateral side, we found that some of these turning components were not active at the same time in both brain hemispheres, but instead were activated differentially depending on whether the fly turned left or right (Fig. 5b).

These data show that part of the globally observed increase in neuronal activity during spontaneous walk corresponds to spontaneous turning behavior. Moreover, components in more than one brain region suggest functional connectivity during turning. As for forward walk, most components could be matched to candidate neurons (Table 2) for future functional analysis.

Brain dynamics at transitions between rest and walk

So far, we have analyzed neuronal activity during walk, turn, flail, groom or resting. Next, we analyzed whole brain activity at the transition between behaviors. As the observed increase in activity appeared during walk, we focused on the transition between rest and walk. Importantly, different GCaMP versions showed equally fast, non-distinguishable onset dynamics. To get a better temporal resolution, we only included datasets recorded at 30 Hz or faster for the entire

brain. We averaged activity at the onset of walk (with a maximum of +/- 30 ms time shift, Fig. S6a). This analysis revealed a more complex picture of neuronal activity with some components being activated significantly before the fly started to walk (Fig. 6). Nevertheless, regardless of the Gal4 line/neuronal type, the recorded whole brain activity showed a significantly higher correlation with walk itself as compared to walk onset or walk offset (see Fig. 1h).

Among the components active before walk onset were several parts of the MB (Fig. 6). Interestingly, while MB-compartment γ4 was active at start of walk, neighboring compartments γ1-3 showed significant activity at ~150-200 ms before the animal started to move. The α2-compartment showed a decrease in activity with walk onset while the α3-compartment became activated ~100 ms after the start of walk (Fig. 6). The β2β'2-compartment of the MB displayed a decrease in neuronal activity starting just before walk. These data are consistent with a role of specific MB-compartments in controlling motor activity (i.e. γ1-3) as well as in integrating walk-related feedback signals (i.e. γ4, α2 and 3, β2β'2; see also [35]). The CL? component in the area of the clamp, surrounding the MB pedunculus in the shape of an interrogation point closely resembles the DNp32 descending neuron [36] (Fig. 6). As this component is activated just after walk initiation, it might be involved in a feedback loop during ongoing behavior. Another brain area previously implicated in movement and navigation is the central complex (e.g., [37]) comprising the protocerebral bridge (PB), fan-shaped body (FB), ellipsoid body (EB), and noduli (NO). Almost all components mapped to these brain areas were activated at walk onset but not before (Fig. 6, S6e) in line with the role of the central complex in navigation and orientation. In particular, the components PB-EB, connecting the PB and the EB, and EB-DA, comprising neurons in the EB and the lateral accessory lobe, became activated once the fly started to walk (Fig. 6, S6e). Of note, the component PB-EB corresponds to the previously described head direction cells shown to receive movement-related information during navigation [38-40]. EB-DA, found in data from dopaminergic neurons, shows among the strongest and most reliable activity during walk. These neurons were shown to be involved in ethanol-induced locomotion [41] and are also involved in sleep regulation [42]. An exception from in the central complex were the ventral layers of the FB (FBlayv, Fig. S6e) and the EB that did not show and increase after walk onset (Fig. 6). Interestingly, the dorsal layer, FBlayd, started to ramp up before walk-onset.This region is involved in arousal and sleep homeostasis [43]. The component in the superior protocerebrum connecting the SLP and SMP region closely resembled a descending neuron, DNp25. In this component and in a couple of other components in the superior protocerebrum, we observed a small, transient increase in neuronal activity before the fly started to walk. This

activity would be consistent with a motor command from the brain to the VNC to initiate walk in some trials. By contrast, another component of this brain region, the medial part of the SMP, SMPm, did not respond to walk at all (Fig. 6). Distinct components mapped to the AVLP displayed very different activities related to walk. While anterior and medial components of AVLP increased in activity at walk onset, the AVLP component that resembled the shape of a shell (AVLPshell) displayed a very clear decrease in neuronal activity as soon as the fly started to walk (Fig. 6).
Several other components displayed more variable, and at times too variable dynamics between flies to detect a clear direction.

To further investigate putative differences in dynamics between neuron types, we next investigated the timing of neuromodulatory regional activity separately relative to walking onset in different brain regions (Fig. S6a-d). Activity before walk onset could be due to top-down motor initiation or possibly preparatory movements that were not detected as walk [44]. Given the suggested importance of DANs for movement preparation and initiation in vertebrates [45], we next analyzed DAN activity more carefully (Fig. S6a). In many brain regions, DAN activity increased at the start of walk (Fig. S6a). In others such as the superior medial protocerebrum (SMP), the activity went up before the fly started to walk and stayed high during walk (Fig. S6a). Some changes in activity occurred after the initiation of walking in octopaminergic neurons (OAN) (Fig. S6b). In most regions, OANs became activated at or just after walk onset displaying an overall very similar picture as seen for cholinergic or inhibitory neurons (Fig. S6b). This was consistent with a study showing a role for octopamine in flight initiation and maintenance [46]. We observed the most interesting and complex activation patterns for serotonergic neurons (Fig. S6c). First, we observed a decrease in activity at walk onset for several brain regions including the AVLP, the PLP, MB calyx (MBCA) and the ICL. However, some regions showed a clear increase at walk onset (e.g., GNG, saddle (SAD) or SIP) (Fig. S6c). We also saw regions where the activity increased initially but decreased quickly after walk onset (e.g. LAL) (Fig. S6c). Aligning the onset of GCaMP fluorescence increases to the onset of walk suggested that the GNG appeared to be activated slightly before the rest of the brain regions responding to walk (Fig. S6f).

While we currently do not understand the biological significance of these different activation patterns in different brain regions, they fit with published neuronal manipulation data, where available, on sleep and motor behavior (see above and discussion). Our data suggest that the

activities of these different types of neurons with distinct functions in state or behavioral control contribute to the global change in brain activity elicited before and during walk. Our analysis provides an entry point to investigate how individual neurons contribute to global brain states and which role this contribution to brain state plays in modulating behavior and sleep.

Forced walk and forced turning recapitulates most activity

Our data suggest that walking induces a change of activity in most of the brain. But where does this activity come from? We hypothesized that in the extreme case, activity could essentially originate from two opposite sites. First, the activity could arise initially in superior decision-making areas and then spread across the brain (top-down) or, second, activity is initiated by motor activity and proprioception (bottom-up) and then distributes to higher brain areas. In the latter case, the activity would originate in the VNC and move to the basal regions of the brain, i.e., the GNG, via ascending neurons (AN) [27]. While our component analysis of data recorded at 30 Hz identified several 'top-down' components active before walk onset, most activity was more consistent with a 'bottom-up' scenario (Fig. 1, 6 and S6). In some trials, we observed that the activity detected during walk appeared to progress from areas at the base of the brain, i.e. GNG to more dorsal areas (see video 6 for an example trial).

We thus asked whether the walk-induced activity could be contributed by axon terminals of ANs. To this end, we expressed a synaptically-tethered GCaMP, syt-GCaMP6, under the control of a pan-neuronal driver and imaged whole brain activity during walk (Fig. 7a). Compared to cellular-GCaMP, syt-GCaMP activity was very strong in the GNG, AMMC and AVLP, the regions receiving input from the VNC (Fig. 7a) [47].

Since such axonal activity, or a fraction of it, could potentially also originate from top-down projections, we carried out another experiment and compared spontaneous, self-induced walk to forced walk (video 3). We argued that if the broad activation indeed comes from proprioception of walking or related sensory input from the legs, we should also observe a global activation when the fly is forced to walk rather than decides to walk spontaneously. To test this idea, we placed a walking substrate controlled by a motor under the fly legs (see Video 6 and methods). We forced the flies to walk by turning this motor on and off at a speed range between 1.5 to 6 mm/s. Spontaneous walk in these flies elicited the typical wholebrain activity as described above (Fig. 7b,d). Remarkably, forced walk also induced a highly similar global activity across the brain (Fig. 7c,d, video 7). Indeed, we found no significant difference in the

correlation coefficient or the R^2-value and regression coefficients across different functional components during spontaneous as compared to forced walk (Fig. 7e,f). In addition, flies with a surgically severed connection between brain and VNC showed hardly any activity in the brain during forced walk (Fig. 7d, video 8) consistent with the hypothesis that whole brain activity is induced by walk itself and originates in the VNC.

Importantly, these observations were not only true for pan-neuronal data but also for dopaminergic, octopaminergic and serotonergic neuronal subsets (Fig. S7a-f). While we did observe some variation between forced and spontaneous walk in the correlation coefficient or the R^2-value for walk, no significant difference was found for any of the brain regions (Fig. S7a-f) further suggesting that walking, whether spontaneous or forced, elicits a highly similar global state change of the brain. By contrast, differences between left and right hemispheres in flies that were forced to turn by 0.3 to 2 radian/s significantly differed from lateral differences in flies that turned spontaneously (Fig. 7g). We subtracted the R^2-value for turn of the contralateral side of the brain from the corresponding value of the ipsilateral side and compared these values for individual components. We found that some components switched sign (i.e., IB and IPS-Y) while other components that showed no lateralization during spontaneous turns showed strong differences for forced turns (i.e., PPM2-VI, SLCtract, PB-DA, Bu-PBl-EB, SPS) (Fig. 7g).

Taken together, these data are consistent with a model wherein a substantial part of the whole brain activity observed during walk is induced by walk itself and/or by walk-related proprioceptive stimulation and not by top-down activity of higher brain centers. As we did not observe a stronger increase in overall brain activity during forced walk as compared to spontaneous walk, our data also suggests that brain activity does not represent a mismatch, or error signal, between actual and predicted proprioceptive feedback during walk. However, more detailed analysis of the lateralization of activity during spontaneous *vs.* forced turns revealed some local differences, which could be consistent with error signals.

Discussion

Work over the last years has revealed that locomotion and movement influence the activity of neurons in many brain areas and organisms [48]. Importantly, motor activity modulates not only local activity in specific brain regions, instead it appears to change the global state of the brain. Where this activity originates from, how it spreads, and what it means for the animal is still debated [49]. Using a tethered fly preparation and fast *in vivo* whole brain imaging, we showed that movement elicits a global change in brain activity during spontaneous as well as forced walk. Our data further suggested that walk activates several different classes of neurons including excitatory (cholinergic) neurons, inhibitory neurons as well as aminergic, modulatory neuron types. With the exception of serotonergic neurons which are inhibited during walk in some brain areas, we observed neuronal activation across all brain regions at the start of and during walking, but not during grooming or resting. Using PCA/ICA transformation, we mapped neuronal activities to discrete functional components, which we assigned to specific smaller subregions and in some cases even to single neurons by aligning the activity data to a comprehensive set of anatomical images and data from different community sources. For instance, we pinpointed specific neurons activated during turning. Based on our data and analysis, we propose that locomotion activates the brain by sending movement and proprioceptive information to the base of the brain (the GNG) from where it activates all brain regions. These data and analysis inspire testable hypotheses and provide a resource of potential neural substrates involved in the perception or control of walking behavior.

Role and origin of broad activation during ongoing behavior

One important concept to explain the role of behavioral state-dependent neural modulation is referred to as ‘Active sensation’ [50]. Essentially, ongoing movement can shape how neurons respond to visual, somatosensory and other sensory stimuli [51]. Our data indicate that whole brain activity is elicited with walk onset and maintained afterwards (see Figure 6). Our analysis furthermore revealed brain areas and select neurons that respond to turning (see Fig. 5). These observations support the conclusion that movement specific, proprioceptive and other sensory information reach the brain and modulate brain activity widely. Such information could serve multiple purposes from uncoupling of sensory-to-motor information, i.e. own movement *vs.* movement of environment, to learning of complex movements. Brainwide neural and glial responses appear to enable behavioral flexibility in zebrafish [52]. By coupling sensory processing and behavior in a closed loop, brain activation during ongoing behavior could resemble a form

of working memory, in part for learning to improve future (motor) behavior or to relate body-movement to environmental information [53].

Our results are most consistent with a model where proprioceptive, walking and leg sensory information are sent from the VNC into the GNG at the base of the fly's brain [54]. This is consistent with extracellular recordings from V1 neurons of mice walking on a ball showed that evoked visual responses differed during movement as compared to neurons of still animals. Similarly, fly visual neurons respond stronger stimuli during active walk or flight [55]. In these studies, and ours, visual information was not required to induce these changes during walk (see Fig. 1). So, how is walking related information relayed to the brain? Tuthill and colleagues recently identified some of the presumably many neural substrates in the VNC that receive, process and relay proprioceptive sensory information from the legs to the CNS [54]. Their findings provide strong support for an important role of proprioception in movement and locomotion control in the adult fly. This information is transmitted by ascending neurons from the VNC to the central brain. So far, relatively little is known regarding the type, connectivity and function of the likely dozens or more ascending neurons in *Drosophila*, but screening approaches and advanced imaging techniques have shed light on some of them [56].

While grooming or forced walk on a treadmill do not require an active brain, lesions of the neck connectives as we have carried out dramatically decrease spontaneous walking in locusts [57] and in flies (see Fig. 7) indicating that at least initiation of walk can be dependent on the brain. On the other hand, a cat with a severed spinal cord, like our fly with a severed VNC, maintains a highly coordinated walk pattern when forced to walk on a treadmill [58]. Thus, coordinated walk appears to mainly depend on central pattern generators in the spinal cord or VNC and is largely independent of brain input. Surprisingly, whole brain activity induced by spontaneous walking was similar to the activity we observed by forcing the animal to walk on a rotating rod (see Fig. 7). This activity disappeared when the connection between VNC and brain was disrupted. It is conceivable that a similar effect would be observed in a cat or a mouse being forced to walk on a treadmill with a severed spinal cord. This result and our finding that the activity first induced by walk in the GNG stems from axons are consistent with the interpretation that walk itself and not top-down motor control is responsible for the majority of activity observed in actively moving animals' brains. We can, however, not exclude that the fly that was forced to walk responded not only with passive rhythmic walking, while also by trying to actively stop and counteract the rotating rod, but this would have engendered a modification in behavior that we did not observe.

Walk elicits differential activities in neuromodulatory neurons

Perhaps not surprisingly, neuromodulatory systems participate and show signatures of ongoing behavior in the adult fly brain (see Fig. 3). Dopaminergic and octopaminergic neurons are broadly activated when the fly walks but not when it grooms (see Fig. 3, [59]), while serotonergic neurons show more complex activation patterns and timing with areas such as the AVLP being inhibited during walk (see Fig. 3 and S6).

Our data suggest that relationships between the activity of neuromodulatory neurons and locomotion are broadly conserved across species. Dopamine neurons are activated during locomotion in mammals, with some neurons reporting ongoing behavior [60] while others are active at behavior onset [61]. We find that although the majority of fly dopamine neurons are activated during ongoing behavior, some dopaminergic neurons are activated milliseconds before the onset of walk (e.g. α2 compartment of the mushroom body, see Fig. 6). Norepinephrine/octopamine is also a key neuromodulatory systems involved in arousal in a variety of species [62], with reports of an increase in activity of these neurons during locomotion in mammals [63-65], also consistent with our observations in flies. Interestingly, serotonergic neurons show mixed roles in the control of motor behavior in different vertebrate species [66, 67], as well as in our fly data. In particular, serotonin has been implicated in behavioral inhibition (e.g. patience) and as an opposing system to dopamine [68, 69]. This is consistent with our observation that serotonergic neurons in the AVLP are inhibited during walk. Similarly, serotonergic neurons in the fly VNC are also inhibited during walking behavior as previously reported [70]. Our study thus suggests that the activity of neuromodulatory neurons during locomotion is conserved between mammals and insects despite their evolutionary distance.

The role of these neuromodulators in locomotion is still debated. In vertebrates, basal ganglia and brainstem aminergic neurons affect the cortico-basal ganglia-thalamic loops. A disruption of these loops can result in a loss of motor control [71]. Such loops likely exist in insects, too. For example, several octopaminergic neurons connect lower brain regions to the MB [72]. Dopaminergic neurons innervate central complex and MB [34]. In line with this, we observe a strong activation of dopaminergic and octopaminergic neurons during walk. Serotonin has varied roles in vertebrates and regulate various types of motor behaviors including feeding, aggression and larval locomotion in insects (e.g., [73]). The AVLP, we identify as a key region where serotonin neurons are inhibited during walk (see Fig. 3 and 6) receives input from

ascending neurons from the VNC conveying somatosensory information from the legs [47]. Interestingly, calcium imaging revealed a spatial map for the AVLP and WED with neurons responding primarily to movement of fore-, mid- or hindlegs [27]. The walk-related role of the strongly inhibited region we termed AVLPshell has not been studied yet, to our knowledge. The functional component maps matched to anatomical templates should thus be helpful in identifying neurons within these regions and their respective functions during walk.

Advantages and limitation of the method

Whole brain connectomics in several small organisms including *Drosophila* has shown that neural networks extend across the entire brain with many pathways not predicted by single neuron or small motif imaging or manipulation of individual neurons [74]. Wholebrain imaging, as previously demonstrated in other model animals such as larval zebrafish, is a powerful method for observing these brainwide networks to study their contribution to behavior and ultimately to local activities within specific neurons or brain regions. Lightfield microscopy has several advantages and limitations, which complement other existing imaging methods. First, the lightfield speed –significantly higher temporal resolution as compared to sequential scanning methods– allowed us to record whole brain activity at the same time as fast behavioral patterns. However, GCaMP dynamics and limitations in signal-to-noise ratio rarely permitted us to resolve single action potentials, so we might be missing important computational aspects. Second, functional units might not be neurons in the fly, but rather micronetworks due to the strong non-synaptic coupling and the many non-spiking neurons. The spatial resolution of lightfield imaging is inferior to that of confocal or volumetric multiphoton imaging. Although these methods do not allow resolving single neurites with pan-neuronally expressed sensors, lightfield could make it even more difficult to detect whether neurites could act as independent functional units. On the other hand, capturing the whole volume simultaneously makes it easier to unmix signals as we showed with our PCA/ICA approach, which partially compensates for the lower spatial resolution. Third, our data is based on observations without genetic or functional manipulation of neurons or circuits. Excitation and inhibition of single neurons are being carried out very frequently in *Drosophila* thanks to its unique genetic tools. We believe that our data complements previous and future functional studies as imaging or manipulation of individual neurons provides only limited insights into the role and effect of a neuron in the complex dynamic neural networks in which they are embedded. Indeed, the response of one neuron relative to the rest of the network is likely to be important (even simplest model neurons integrate activity from several input neurons in a timely fashion). In the future, a combination of

single neuron manipulation and wholebrain imaging will likely lead to unexpected insights into the relationship of a neuron and a specific behavior. Fourth, we have observed subtler differences between flies that are obvious from individual experiments but difficult to capture quantitatively across a population of animals. These subtle differences might be resolvable by greatly increasing the number of experiments. Given the technical difficulty of the preparation method, reaching high animal numbers will be extremely challenging but perhaps possible in the future. Finally, together with the now available wholebrain EM connectome, our data provides a timely resource for the community of fly neuroscientists interested in linking neuronal activity to behavior.

Conclusions

We provide an overview of brain activity during simple behaviors in *Drosophila*. As for other animals, *Drosophila* brain activity is globally correlated with locomotion leading to global change in brain state. However, our results challenge the assumption that most of the activity is related to decision-making, top-down motor control, or prediction error detection from sensory feedback and instead suggest that walk itself and somatosensory bottom-up stimuli are largely responsible. By using a combination of pan-neuronal and specific neuron line imaging, we shed light on the nature of neurons and their location in the brain that respond so strongly to behavior. Altogether, our data provide a novel resource for further generating new hypotheses regarding the brain-behavior-loop and for dissecting the neural circuits underpinning it.

Author contributions

SA developed the preparation, made the initial observation, and generated most data sets. KC generated additional datasets. SA analyzed the data with the help of KC. JG and IGK oversaw the study. SA and IGK wrote the paper with help and input by all other authors.

Acknowledgments

We are very grateful to Marta Costa and Kei Ito for sharing data, images, and knowledge during the course of this study. We also thank Francisco Rodriguez-Jimenez, Paul Bandow, Subhadarshini Parhi and Kunhi Purayil Siju for help with data analysis.

Conflict of Interest

The authors declare no conflict of interest.

Supplementary Information

Supplementary figures S1 to S7

Table 1: ANOVA analysis of regression R^2 for brain activity vs. different types of behavior and for different pan-neuronal expression genotypes

Table 2: List of all reproducibly identified components correlated with walk and additional information including putative neurons.

Video files

Video 1: Movie of pan-neuronal activation during walk and groom (accelerated).

Video 2: Movie of TH/DDC-neuronal activation during walk (accelerated).

Video 3: Movie of TDC2-neuronal activation during walk (accelerated).

Video 4: Movie of Trh-neuronal activation during walk (accelerated).

Video 5: Video sequence showing activation of the PPM2-LW neurons during turning.

Video 6: Video showing neuronal activation moving from ventral to dorsal brain areas. Note that a clear progression of activation was observed only in a fraction of trials.

Video 7: Video showing whole brain activity of a fly being forced to walk on a rotating rod.

Video 8: Video showing whole brain activity of a fly with a severed connection between brain and VNC being forced to walk on a rotating rod. Note that the fly is still capable of walking on the rod when being forced. We did, however, not observe spontaneous walking activity.

Materials and Methods

RESOURCE AVAILABILITY

Further information and requests for resources should be directed to Ilona Grunwald Kadow (Ilona.grunwald@uni-bonn.de).

Materials availability

This study did not generate new unique reagents.

Data and code availability

All original code has been deposited at Github and is publicly available. Original data and any additional information required to reanalyze the data reported in this paper are available upon request.

MATERIALS

Deposited data		
Example dataset with raw data	CNCRS	https://crcns.org/data-sets/ia/fly-1/about-fly-1
Processed data for figures	GitHub	https://github.com/sophie63/Aimon2022
All other data is available upon request		
Experimental models: Organisms/strains		
UAS-GCaMP6s	Bloomington Drosophila Stock Center	BDSC_42749
UAS-GCaMP6m	Bloomington Drosophila Stock Center	BDSC_42750
UAS-GCaMP7s	Bloomington Drosophila Stock Center	BDSC_79032
UAS-GCaMP6f	Bloomington Drosophila Stock Center	BDSC_42747
UAS-GCaMP7f	Bloomington Drosophila Stock Center	BDSC_79031
UAS-syt-GCaMP6s	Vanessa Ruta	N/A
GMR58E02-Gal4	Bloomington Drosophila Stock Center	BDSC_41347
Th-Gal4	Bloomington Drosophila Stock Center	BDSC_8848

Tdc2-Gal4	Bloomington Drosophila Stock Center	BDSC_9313
Trh-Gal4	Bloomington Drosophila Stock Center	BDSC_38388
Ddc-Gal4	Bloomington Drosophila Stock Center	BDSC_7009
TH, 58E02-Gal4	Siju et al.	N/A
TH, DDC-Gal4	This paper	N/A
Vglut-Gal4	Bloomington Drosophila Stock Center	BDSC_24635
Cha-Gal4	Bloomington Drosophila Stock Center	BDSC_6798
Nsyb-Gal4	Bloomington Drosophila Stock Center	BDSC_51635
GMR57C10-Gal4	Bloomington Drosophila Stock Center	BDSC_39171
Gad1-Gal4	Bloomington Drosophila Stock Center	BDSC_51630
Software and algorithms		
Python 3	Python Software Foundation	https://www.python.org
ImageJ	Schneider et al., 2012	https://imagej.nih.gov/ij/
Fiji	MPI-CBG	https://fiji.sc/
MATLAB	MATLAB	mathworks.com
Analysis code	GitHub	https://github.com/sophie63/Aimon2022

EXPERIMENTAL MODEL AND SUBJECT DETAILS

Drosophila melanogaster

We used one to four days old female flies raised at 25 °C. Most flies were starved 24 or 48h with a water only environment, and we clipped the wings at least one day in advance. Experiments were performed in the evening peak of circadian activity (ZT0 or ZT11) and we heated the room to ~28 °C during the experiment. In total, we recorded brain activity and behavior from 84 adult female flies.

METHOD DETAILS

Fly preparation for imaging

We prepared the flies as described in detail in [14]. Briefly, we fixed a fly to a custom-designed 3D printed holder, so as to allow access to the whole posterior side of the head while the legs were free to move. We added saline (103 mM NaCl, 3 mM KCl, 5 mM TES, 8 mM trehalose 2 H_2O, 10 mM glucose, 26 mM $NaHCO_3$, 1 mM NaH_2PO_4, 2.5 mM $CaCl_2 \cdot 2\ H_2O$, 4 mM $MgCl_2 \cdot 6\ H_2O$) and dissected the cuticle, muscles, and air sacks at the back of the head to expose the brain.

Walk substrates

For studying spontaneous walk, we used two types of small balls. One was an air-supported ball as previously described [15]. As we wanted to make sure the walk was initiated by the fly rather than erratic movement of the ball, we also used small styrofoam balls that were held by the fly. In addition, the posture of flies on a held Styrofoam ball was more natural than on the air-supported ball. In both preparations, flies walked spontaneously, and the brain activity elicited by spontaneous walk was not significantly different between the s. Therefore, these data were combined in all analysis.

As treadmill for studying forced walk and turn, we used small motors (DC 6V gear motor with long M3 x 55mm lead screw thread output shaft speed reducer Walfront Store, www.amazon.de), covered with self-curing rubber (from Sugru) to provide a smoother surface. The speed for forced walk was between 1.5 and 6 mm/s. The rotation speed for forced turn was 0.3 to 2 rad/s.

In vivo lightfield imaging

Fast volumetric imaging was performed using lightfield imaging – in which a microlens array separates rays- from different angles to give information on depth -- was carried out as previously described in detail by [8]. A few datasets were previously published in Aimon et al. [8] and source data (http://dx.doi.org/10.6080/K01J97ZN), with a microscope equipped with a 20x NA1.0 objective. Most data were obtained with a lightfield microscope constituted of a Thorlabs Cerna system with a Leica HC FLUOTAR L 25x/0.95 objective and an MLA-S125-f12 microlens array (Viavi). The microlens array was placed on the image plane, while the camera imaged the microlens array through 50 mm f/1.4 NIKKOR-S Nikon relay lenses. The light field images were recorded with a scientific CMOS camera (Hamamatsu ORCA-Flash 4.0). The volumes were reconstructed offline, using a python program developed by [75] and available on github: https://github.com/sophie63/FlyLFM.

Given that the maximum recording speed depended on the expression of the Gal4-line, the UAS-reporter, and each individual fly preparation, i.e. the limiting factor was the signal-to-noise ratio for lines with low expression, we always started recording at 2 or 5 Hz for the first experiment. If the quality of recording suggested that higher speeds were possible, we increased recording speed stepwise to a maximum of 98 Hz. If the viability of the fly allowed for it, we recorded experiments on air-supported and Styrofoam balls in the same fly.

Gal4	UAS - GCaMP	# of flies, spontaneous Walk (flail, groom)	flailing	grooming	frame rate in Hz (# of experiments)	Walking Substrate (# of experiments)	# flies of flies forced walk
total	**total**	**58**	9	6	98(8), 50(21), 20(11), 10(9), 5(30), 2(2)	Air-supported ball (33), styrofoam ball (54)	**26**
Nsyb	7f	1	1	1	50(1)	Air-supported ball	
	7s	1	1		5(1)	styrofoam ball	1
	6m	6	5	2	50(8), 20(5), 10(3), 5(4)	Air-supported ball (16), styrofoam ball (5)	3
	6f	3		1	98(2), 50(1)	Air-supported ball (2), styrofoam ball (1)	
	6s	1	1		50(1)	styrofoam ball(1)	2
	total	12	8	4	98(2), 50(11), 20(5), 10(3), 5(5)	Air-supported ball (19), styrofoam ball (8)	6
R57C10	7s	1		1	98(2)	styrofoam ball(2)	
	6s	3	1	1	50(1), 5(1), 20(1)	styrofoam ball(3)	3
	total	4	1	2	98(2), 50(1), 20(1), 5(1)	Air-supported ball (0), styrofoam ball (5)	3
Cha	6m	4			5(4)	styrofoam ball (4)	
	6f	1			98(1)	Air-supported ball (1)	
	total	5			98(1), 5(4)	Air-supported ball (1), styrofoam ball (4)	0
Vglut	6m	5			20(2), 10(3), 5(4)	Air-supported ball (3), styrofoam ball (6)	

	total	5			20(2), 10(3), 5(4)	Air-supported ball (3), styrofoam ball (6)	0
Gad	6m	5			98(2), 20(1), 5(5), 2(1)	styrofoam ball (9)	
	total	5			98(2), 20(1), 5(5), 2(1)	Air-supported ball (0), styrofoam ball (9)	0
TH/DDC	6m	5			50(2), 5(1), 10(1)	Air supported ball (3), styrofoam ball (2)	4
	6f	6			50(5), 98(1)	Air supported ball (2), styrofoam ball (3)	1
	total	11			98(1), 50(7), 10(1), 5(1)	Air-supported ball (5), styrofoam ball (5)	5
Trh	6m	3			50(3), 5(3)	Air supported ball (1), styrofoam ball (6)	
	6f	3			10(2)	Air supported ball (2), styrofoam ball (1)	
	6s	3			5(3)	styrofoam ball(4)	6
	total	9			50(3), 10(2), 5(6)	Air-supported ball (3), styrofoam ball (11)	6
Tdc2	6s	7			20(2), 5(4), 2(1)	Air supported ball (2), styrofoam ball (6)	6
	total	7			20(2), 5(4), 2(1)	Air-supported ball (2), styrofoam ball (6)	6

Behavior recording and scoring

We imaged the fly and substrate movements using infra-red illumination and two small cameras FFMV-03M2M from Point Grey triggered by the fluorescence recording camera to ensure time alignment between fluorescence and behavior.

Walking, flailing, and grooming were obtained by measuring the optic flow from the videos of the ball or by analyzing the movement of the fly's legs using the "optic flow" plugin in FIJI. For turning or rotational speed (rad/s), the sum of left or right optic flows was not binarized. The behavioral time series were then convolved with the single spike response of the GCaMP version used for the experiment and subjected to the same deltaF/F procedure as the fluorescence time series (see below).

Pre-processing

Reconstructed volumetric fluorescence data was pre-processed by first correcting for movement using 3Dvolreg from AFNI [76]. In Matlab, we then calculated the deltaF/F for each voxel by subtracting and dividing by the signal averaged for 4000 time points. We finally decreased noise with a Kalman filter (from https://www.mathworks.com/matlabcentral/fileexchange/26334-kalman-filter-for-noisy-movies) with a gain of 0.5.

We generated summary movies by maximum projecting the $\Delta F/F$ volumes and combining these to the behavior.

Alignment to template

We aligned the functional data to anatomical templates using landmarks registration with ImageJ (as described in http://imagej.net/Name_Landmarks_and_Register).

STATISTICAL ANALYSIS

Statistics were performed in python with code freely available on https://github.com/sophie63/Aimon2022. To compare fluorescence time series (normalized by the absolute maximum value per fly) and behavioral time series, we used a simple regression model: TSfluo ~ BehaviorRegressor, solved with the ordinary least square fit function of the python statsmodels package. For each time series (either regional averaged intensity or the PCA/ICA component), this provided a fraction of variance explained by the behavior (R^2), and the sign and strength of the correlation (coefficient). We compared these values with pair-wise tests using two-sided Mann-Whitney non-parametric tests with a Bonferroni multiple comparison correction. Flies were recorded over prolonged periods of times at different imaging speeds and during different behaviors. See table above for details on number of individual flies and types of experiments per fly.

We used a linear model to evaluate the effect of variables of interest (behavior, brain region, neural type) while explaining away confounds (GCaMP version, exact pan neuronal Gal4): R2 ~ Behavior+RegionNames+Gal4+UAS and Coef ~ Behavior+RegionNames+Gal4+UAS. We then plotted the coeffcients + intercept, and 95% interval of coefficient + 95% interval of the intercept to compare the effect of the variables to zero.

PCA/ICA

To obtain functional maps of the fly brain, we performed PCA and ICA as described previously [77]. Briefly, SVD (singular value decomposition) was used a first time to find the level of noise and normalize voxels by their noise variance. SVD was performed a second time on this normalized data resulting in maps and time series for principal components. The principal component maps were unmixed using ICA to obtain localized regions. The same matrix was used to unmix the time series.

The functional regions were aligned with anatomical templates as described above. This allowed finding the anatomically defined regions covered by the functional regions (see Table 2) and find candidate neurons (using Flycircuit (http://www.flycircuit.tw/) or Virtual Fly Brain https://v2.virtualflybrain.org) data bases).

References

1. Parker, P.R.L., Brown, M.A., Smear, M.C. & Niell, C.M. Movement-Related Signals in Sensory Areas: Roles in Natural Behavior. *Trends Neurosci* **43**, 581-595 (2020).
2. Kaplan, H.S. & Zimmer, M. Brain-wide representations of ongoing behavior: a universal principle? *Curr Opin Neurobiol* **64**, 60-69 (2020).
3. Mace, E.*, et al.* Whole-Brain Functional Ultrasound Imaging Reveals Brain Modules for Visuomotor Integration. *Neuron* **100**, 1241-1251 e1247 (2018).
4. Stringer, C.*, et al.* Spontaneous behaviors drive multidimensional, brainwide activity. *Science* **364**, 255 (2019).
5. Musall, S., Kaufman, M.T., Juavinett, A.L., Gluf, S. & Churchland, A.K. Single-trial neural dynamics are dominated by richly varied movements. *Nat Neurosci* **22**, 1677-1686 (2019).
6. Kato, S.*, et al.* Global brain dynamics embed the motor command sequence of Caenorhabditis elegans. *Cell* **163**, 656-669 (2015).
7. Dunn, T.W.*, et al.* Brain-wide mapping of neural activity controlling zebrafish exploratory locomotion. *Elife* **5**, e12741 (2016).
8. Andalman, A.S.*, et al.* Neuronal Dynamics Regulating Brain and Behavioral State Transitions. *Cell* **177**, 970-985 e920 (2019).
9. Maimon, G., Straw, A.D. & Dickinson, M.H. Active flight increases the gain of visual motion processing in Drosophila. *Nat Neurosci* **13**, 393-399 (2010).
10. Fujiwara, T., Cruz, T.L., Bohnslav, J.P. & Chiappe, M.E. A faithful internal representation of walking movements in the Drosophila visual system. *Nat Neurosci* **20**, 72-81 (2017).
11. Siju, K.P.*, et al.* Valence and State-Dependent Population Coding in Dopaminergic Neurons in the Fly Mushroom Body. *Curr Biol* **30**, 2104-2115 e2104 (2020).
12. Zolin, A.*, et al.* Context-dependent representations of movement in Drosophila dopaminergic reinforcement pathways. *Nat Neurosci* **24**, 1555-1566 (2021).
13. Aimon, S.*, et al.* Fast near-whole-brain imaging in adult Drosophila during responses to stimuli and behavior. *PLoS Biol* **17**, e2006732 (2019).
14. Schaffer, E.S.*, et al.* Flygenvectors: The spatial and temporal structure of neural activity across the fly brain. *bioRxiv*, 2021.2009.2025.461804 (2021).
15. Scheffer, L.K.*, et al.* A connectome and analysis of the adult Drosophila central brain. *Elife* **9** (2020).

16. Berman, G.J., Bialek, W. & Shaevitz, J.W. Predictability and hierarchy in Drosophila behavior. *Proc Natl Acad Sci U S A* **113**, 11943-11948 (2016).
17. Calhoun, A.J., Pillow, J.W. & Murthy, M. Author Correction: Unsupervised identification of the internal states that shape natural behavior. *Nat Neurosci* (2019).
18. DeAngelis, B.D., Zavatone-Veth, J.A. & Clark, D.A. The manifold structure of limb coordination in walking Drosophila. *Elife* **8** (2019).
19. Geurten, B.R., Jahde, P., Corthals, K. & Gopfert, M.C. Saccadic body turns in walking Drosophila. *Front Behav Neurosci* **8**, 365 (2014).
20. Katsov, A.Y., Freifeld, L., Horowitz, M., Kuehn, S. & Clandinin, T.R. Dynamic structure of locomotor behavior in walking fruit flies. *Elife* **6** (2017).
21. Mendes, C.S., Rajendren, S.V., Bartos, I., Marka, S. & Mann, R.S. Kinematic responses to changes in walking orientation and gravitational load in Drosophila melanogaster. *PLoS One* **9**, e109204 (2014).
22. Mueller, J.M., Ravbar, P., Simpson, J.H. & Carlson, J.M. Drosophila melanogaster grooming possesses syntax with distinct rules at different temporal scales. *PLoS Comput Biol* **15**, e1007105 (2019).
23. Tao, L., Ozarkar, S., Beck, J.M. & Bhandawat, V. Statistical structure of locomotion and its modulation by odors. *Elife* **8** (2019).
24. Tsai, K.T. & Chou, Y.H. Random Walk Revisited: Quantification and Comparative Analysis of Drosophila Walking Trajectories. *iScience* **19**, 1145-1159 (2019).
25. Zacarias, R., Namiki, S., Card, G.M., Vasconcelos, M.L. & Moita, M.A. Speed dependent descending control of freezing behavior in Drosophila melanogaster. *Nat Commun* **9**, 3697 (2018).
26. von Philipsborn, A.C*., et al.* Neuronal control of Drosophila courtship song. *Neuron* **69**, 509-522 (2011).
27. Emanuel, S., Kaiser, M., Pflueger, H.J. & Libersat, F. On the Role of the Head Ganglia in Posture and Walking in Insects. *Front Physiol* **11**, 135 (2020).
28. Bidaye, S.S*., et al.* Two Brain Pathways Initiate Distinct Forward Walking Programs in Drosophila. *Neuron* **108**, 469-485 e468 (2020).
29. Bidaye, S.S., Machacek, C., Wu, Y. & Dickson, B.J. Neuronal control of Drosophila walking direction. *Science* **344**, 97-101 (2014).
30. Schilling, M. & Cruse, H. Decentralized control of insect walking: A simple neural network explains a wide range of behavioral and neurophysiological results. *PLoS Comput Biol* **16**, e1007804 (2020).
31. Sims, D.W., Humphries, N.E., Hu, N., Medan, V. & Berni, J. Optimal searching behaviour generated intrinsically by the central pattern generator for locomotion. *Elife* **8** (2019).
32. Woller, A., Bandow, P., Aimon, S. & Grunwald Kadow, I.C. Preparing Adult Drosophila melanogaster for Whole Brain Imaging during Behavior and Stimuli Responses. *J Vis Exp* (2021).
33. Sayin, S*., et al.* A Neural Circuit Arbitrates between Persistence and Withdrawal in Hungry Drosophila. *Neuron* **104**, 544-558 e546 (2019).
34. Seelig, J.D*., et al.* Two-photon calcium imaging from head-fixed Drosophila during optomotor walking behavior. *Nat Methods* **7**, 535-540 (2010).
35. Hampel, S., Franconville, R., Simpson, J.H. & Seeds, A.M. A neural command circuit for grooming movement control. *Elife* **4**, e08758 (2015).
36. Borst, A., Haag, J. & Mauss, A.S. How fly neurons compute the direction of visual motion. *J Comp Physiol A Neuroethol Sens Neural Behav Physiol* **206**, 109-124 (2020).
37. Suver, M.P., Huda, A., Iwasaki, N., Safarik, S. & Dickinson, M.H. An Array of Descending Visual Interneurons Encoding Self-Motion in Drosophila. *J Neurosci* **36**, 11768-11780 (2016).

38. Creamer, M.S., Mano, O. & Clark, D.A. Visual Control of Walking Speed in Drosophila. *Neuron* **100**, 1460-1473 e1466 (2018).
39. Sen, R., Wang, K. & Dickson, B.J. TwoLumps Ascending Neurons Mediate Touch-Evoked Reversal of Walking Direction in Drosophila. *Curr Biol* **29**, 4337-4344 e4335 (2019).
40. Hsu, C.T. & Bhandawat, V. Organization of descending neurons in Drosophila melanogaster. *Sci Rep* **6**, 20259 (2016).
41. Benjamin, P.R., Staras, K. & Kemenes, G. What roles do tonic inhibition and disinhibition play in the control of motor programs? *Front Behav Neurosci* **4**, 30 (2010).
42. Tsubouchi, A.*, et al.* Topological and modality-specific representation of somatosensory information in the fly brain. *Science* **358**, 615-623 (2017).
43. Chen, C.-L.*, et al.* Ascending neurons convey behavioral state to integrative sensory and action selection centers in the brain. *bioRxiv*, 2022.2002.2009.479566 (2022).
44. Li, Y.*, et al.* The Role of Monoaminergic Neurotransmission for Metabolic Control in the Fruit Fly Drosophila Melanogaster. *Front Syst Neurosci* **11**, 60 (2017).
45. Cohn, R., Morantte, I. & Ruta, V. Coordinated and Compartmentalized Neuromodulation Shapes Sensory Processing in Drosophila. *Cell* **163**, 1742-1755 (2015).
46. Liu, C.*, et al.* A subset of dopamine neurons signals reward for odour memory in Drosophila. *Nature* **488**, 512-516 (2012).
47. Lee, Y.J.*, et al.* Conservation and divergence of related neuronal lineages in the Drosophila central brain. *Elife* **9** (2020).
48. Chiang, A.S.*, et al.* Three-dimensional reconstruction of brain-wide wiring networks in Drosophila at single-cell resolution. *Curr Biol* **21**, 1-11 (2011).
49. Coates, K.E.*, et al.* The Wiring Logic of an Identified Serotonergic Neuron That Spans Sensory Networks. *J Neurosci* **40**, 6309-6327 (2020).
50. Namiki, S., Dickinson, M.H., Wong, A.M., Korff, W. & Card, G.M. The functional organization of descending sensory-motor pathways in Drosophila. *Elife* **7** (2018).
51. Robie, A.A.*, et al.* Mapping the Neural Substrates of Behavior. *Cell* **170**, 393-406 e328 (2017).
52. Cande, J.*, et al.* Optogenetic dissection of descending behavioral control in Drosophila. *Elife* **7** (2018).
53. Mao, Z. & Davis, R.L. Eight different types of dopaminergic neurons innervate the Drosophila mushroom body neuropil: anatomical and physiological heterogeneity. *Front Neural Circuits* **3**, 5 (2009).
54. Seelig, J.D. & Jayaraman, V. Feature detection and orientation tuning in the Drosophila central complex. *Nature* **503**, 262-266 (2013).
55. Lyu, C., Abbott, L.F. & Maimon, G. Building an allocentric travelling direction signal via vector computation. *Nature* **601**, 92-97 (2022).
56. Ache, J.M., Namiki, S., Lee, A., Branson, K. & Card, G.M. State-dependent decoupling of sensory and motor circuits underlies behavioral flexibility in Drosophila. *Nat Neurosci* **22**, 1132-1139 (2019).
57. Azanchi, R., Kaun, K.R. & Heberlein, U. Competing dopamine neurons drive oviposition choice for ethanol in Drosophila. *Proc Natl Acad Sci U S A* **110**, 21153-21158 (2013).
58. Brembs, B., Christiansen, F., Pfluger, H.J. & Duch, C. Flight initiation and maintenance deficits in flies with genetically altered biogenic amine levels. *J Neurosci* **27**, 11122-11131 (2007).
59. Busse, L.*, et al.* Sensation during Active Behaviors. *J Neurosci* **37**, 10826-10834 (2017).
60. Chapman, P.D.*, et al.* Flight motor networks modulate primary olfactory processing in the moth Manduca sexta. *Proc Natl Acad Sci U S A* **115**, 5588-5593 (2018).
61. Henschke, J.U., Price, A.T. & Pakan, J.M.P. Enhanced modulation of cell-type specific neuronal responses in mouse dorsal auditory field during locomotion. *Cell Calcium* **96**, 102390 (2021).

62. Haesemeyer, M., Robson, D.N., Li, J.M., Schier, A.F. & Engert, F. A Brain-wide Circuit Model of Heat-Evoked Swimming Behavior in Larval Zebrafish. *Neuron* **98**, 817-831 e816 (2018).
63. Fu, Y.*, et al.* A cortical circuit for gain control by behavioral state. *Cell* **156**, 1139-1152 (2014).
64. Fenk, L.M., Kim, A.J. & Maimon, G. Suppression of motion vision during course-changing, but not course-stabilizing, navigational turns. *Curr Biol* (2021).
65. Cruz, T.L., Perez, S.M. & Chiappe, M.E. Fast tuning of posture control by visual feedback underlies gaze stabilization in walking Drosophila. *Curr Biol* (2021).
66. Wolpert, D.M., Diedrichsen, J. & Flanagan, J.R. Principles of sensorimotor learning. *Nat Rev Neurosci* **12**, 739-751 (2011).
67. Mu, Y.*, et al.* Glia Accumulate Evidence that Actions Are Futile and Suppress Unsuccessful Behavior. *Cell* **178**, 27-43 e19 (2019).
68. Lu, J.*, et al.* Transforming representations of movement from body- to world-centric space. *Nature* (2021).
69. Mamiya, A., Gurung, P. & Tuthill, J.C. Neural Coding of Leg Proprioception in Drosophila. *Neuron* **100**, 636-650 e636 (2018).
70. Agrawal, S.*, et al.* Central processing of leg proprioception in Drosophila. *Elife* **9** (2020).
71. Chiappe, M.E., Seelig, J.D., Reiser, M.B. & Jayaraman, V. Walking modulates speed sensitivity in Drosophila motion vision. *Curr Biol* **20**, 1470-1475 (2010).
72. Allen, A.M.*, et al.* A single-cell transcriptomic atlas of the adult Drosophila ventral nerve cord. *Elife* **9** (2020).
73. Chen, C.L.*, et al.* Imaging neural activity in the ventral nerve cord of behaving adult Drosophila. *Nat Commun* **9**, 4390 (2018).
74. Kien, J. Neuronal activity during spontaneous walking--II. Correlation with stepping. *Comparative biochemistry and physiology. A, Comparative physiology* **95**, 623-638 (1990).
75. Kien, J. Neuronal activity during spontaneous walking--I. Starting and stopping. *Comparative biochemistry and physiology. A, Comparative physiology* **95**, 607-621 (1990).
76. Berry, J.A., Cervantes-Sandoval, I., Chakraborty, M. & Davis, R.L. Sleep Facilitates Memory by Blocking Dopamine Neuron-Mediated Forgetting. *Cell* **161**, 1656-1667 (2015).
77. Collins, L., Boddington, L., Steffan, P.J. & McCormick, D. Vagus nerve stimulation induces widespread cortical and behavioral activation. *Curr Biol* **31**, 2088-2098 e2083 (2021).
78. Reimer, J.*, et al.* Pupil fluctuations track rapid changes in adrenergic and cholinergic activity in cortex. *Nat Commun* **7**, 13289 (2016).
79. Tantirigama, M.L.S., Zolnik, T., Judkewitz, B., Larkum, M.E. & Sachdev, R.N.S. Perspective on the Multiple Pathways to Changing Brain States. *Front Syst Neurosci* **14**, 23 (2020).
80. Vicente, A.M., Martins, G.J. & Costa, R.M. Cortico-basal ganglia circuits underlying dysfunctional control of motor behaviors in neuropsychiatric disorders. *Curr Opin Genet Dev* **65**, 151-159 (2020).
81. Busch, S., Selcho, M., Ito, K. & Tanimoto, H. A map of octopaminergic neurons in the Drosophila brain. *J Comp Neurol* **513**, 643-667 (2009).
82. Flaive, A., Fougere, M., van der Zouwen, C.I. & Ryczko, D. Serotonergic Modulation of Locomotor Activity From Basal Vertebrates to Mammals. *Front Neural Circuits* **14**, 590299 (2020).
83. Vitrac, C. & Benoit-Marand, M. Monoaminergic Modulation of Motor Cortex Function. *Front Neural Circuits* **11**, 72 (2017).
84. Aonuma, H. Serotonergic control in initiating defensive responses to unexpected tactile stimuli in the trap-jaw ant Odontomachus kuroiwae. *J Exp Biol* **223** (2020).

85. Ngai, M., Shoue, D.A., Loh, Z. & McDowell, M.A. The pharmacological and functional characterization of the serotonergic system in Anopheles gambiae and Aedes aegypti: influences on flight and blood-feeding behavior. *Sci Rep* **9**, 4421 (2019).
86. Schoofs, A., Huckesfeld, S. & Pankratz, M.J. Serotonergic network in the subesophageal zone modulates the motor pattern for food intake in Drosophila. *J Insect Physiol* **106**, 36-46 (2018).
87. Helfrich-Förster, C. Sleep in Insects. *Annu Rev Entomol* **63**, 69-86 (2018).
88. Schoofs, A., Huckesfeld, S., Surendran, S. & Pankratz, M.J. Serotonergic pathways in the Drosophila larval enteric nervous system. *J Insect Physiol* **69**, 118-125 (2014).
89. Scheffer, L.K.*, et al.* A connectome and analysis of the adult. *Elife* **9** (2020).
90. Li, F.*, et al.* The connectome of the adult Drosophila mushroom body provides insights into function. *Elife* **9** (2020).
91. Zheng, Z.*, et al.* A Complete Electron Microscopy Volume of the Brain of Adult Drosophila melanogaster. *Cell* **174**, 730-743 e722 (2018).
92. Broxton, M.*, et al.* Wave optics theory and 3-D deconvolution for the light field microscope. *Optics express* **21**, 25418-25439 (2013).
93. Cox, R.W. & Jesmanowicz, A. Real-time 3D image registration for functional MRI. *Magn Reson Med* **42**, 1014-1018 (1999).
94. Beckmann, K.M.*, et al.* Resting state networks of the canine brain under sevoflurane anaesthesia. *PLoS One* **15**, e0231955 (2020).
95. Ito, K.*, et al.* A systematic nomenclature for the

Figure legends

Figure 1: Global brain activation during walk.

(**a**) Schematic overview of the preparation and analysis method. Please see methods for details. (**b**) Raster plot of the activity of regions. Top panels depict walking bouts in green and rest or grooming in magenta. Lower panel shows calcium activity elicited throughout the experiment. The brighter the higher the calcium transients. Mean forward speed: 5.6 mm/s, mean angular velocity: 0.4 radian/s (**c**) Sample traces (deltaF/F) for different brain regions relative to forward walk (green). (**d**) First two principal components from whole brain activity color-coded with behavior. (**e**) R^2 for different behavioral conditions (all regions were pooled, but p-values are obtained after averaging regions for each fly. Walk: N=16, Flail: N=7, Groom: N=6). P-values: Walk vs. Flail 0.085, Walk vs. Groom: 0.011, Flail vs. Groom: 0.26. Center line, median; box limits, upper and lower quartiles; whiskers, 1.5x interquartile range; points, outliers (**f**) Z-stack map of R^2 median (Walk: N (flies) =16, Flail: N=7, Groom: N=6) for regression between regional activity and walk, flail or groom. Mann-Whitney-test: walk vs. flail: 85, walk vs. groom: 85; flail vs. groom: 31 (**g**) Normalized coefficient of different regions' activity regression with walk. All regions' 95% CI are above zero. N=16. (**h**) R^2-value of regression coefficients during walk, walk onset and walk offset (all regions were pooled, nsyb-Gal4: N=16, GMR57C10-Gal4: N=4). Regressors for walk onset or offset are Dirac functions convolved with the GCaMP response. Box plots show: center line, median; box limits, upper and lower quartiles; whiskers, 1.5x interquartile range; points, outliers.

Figure 2: Activity of neurons releasing the three major neurotransmitters, glutamate, GABA and acetylcholine during walk.

(**a**) R^2 for regression of activity with walk in different conditions (all regions were pooled). No pairwise comparison is significantly different. Mann-Whitney-test: Cha vs. GAD: 4; Cha vs. Vglut: 15; GAD vs. Vglut: 22 (**b**) Overview of major brain regions as defined in [78]. (**c**) Activity maps (regression coefficient) of functional regions activated during walk for Cha-Gal4, GAD-Gal4 and Vglut-Gal4 expressing neurons. (**d**) Sample traces (deltaF/F) for different brain regions relative to forward walk (green). (**e**) R^2 of regression of fluorescence vs. walk for Cha-Gal4, GAD-Gal4 and Vglut-Gal4 expressing excitatory neurons. N=5 flies for each individual genotype. Box plots show: center line, median; box limits, upper and lower quartiles; whiskers, 1.5x interquartile range; points, outliers.

Figure 3: Neuromodulatory neurons are strongly and differentially activated during walk. (**a**) Coefficient of determination for behavior regression at different conditions (all regions were pooled). Mann-Whitney-test; P-values: TH vs. Trh: 47, 0.032, TH vs. TDC: 35, ns, Trh vs. TDC: 5, 0.040 (**b**) Activity maps (regression coefficient) of functional regions activated during walk for TH-gal4 and DDC-gal4 or GMR58E04-Gal4 (dopaminergic neurons), TDC2-gal4 (octopaminergic neurons) and Trh-Gal4 (serotoninergic neurons) expressing neurons. Blue indicates inhibition. (**c**) Overlay of activity maps of two neuromodulators in each panel. (**d**) Sample traces (deltaF/F) for different brain regions relative to forward walk (green). (**e**) Coefficient during walk for different brain regions for Trh-Gal4 expressing serotonergic neurons. All regions are significantly correlated. (**f**) R^2 of regression of fluorescence vs. walk for TH/DDC(58E02)-Gal4, Tdc2-Gal4 and Trh-Gal4 expressing excitatory neurons. TH/DDC-Gal4: N=9, Tdc2-Gal4: N=7, Trh-Gal4: N=6 flies. Box plots show: center line, median; box limits, upper and lower quartiles; whiskers, 1.5x interquartile range; points, outliers.

Figure 4: Whole brain analysis pinpoints specific subregions responding to walk. (**a**) Images of example components that are significantly correlated with walk (Coefficient or R^2 95% CI above zero). Upper left: components derived from imaging with a pan-neuronal driver. Upper right: components derived with Tdc2-Gal4. Lower left: components derived with TH/DDC or GMR58E02-Gal4. Lower right: components derived with Trh-Gal4. (**b**) Correlation coefficient for components activity vs walk. N=58 flies of different genotypes, see table in methods for details.

Figure 5: Turning activates specific components and neurons. (**a**) Examples of components present in both the left and right hemisphere labeled in different colors (magenta and green). Panels on the right present an example component that could be mapped to a single neuron. Upper right panel: Turning-correlated component, lower right panel: reconstruction of neuron that this functional component was mapped to. (**b**) Difference between the correlation coefficient (normalized $\Delta F/F$) for turning on the ipsilateral side and the coefficient on the contralateral side is displayed as a function of the identified components. Positive and negative correlations correspond to components being active more during turn on the ipsi-lateral side than the contra-lateral side and the reverse, respectively. See Table 2 for definition of acronyms. N=58 flies of different genotypes, see table in methods for details.

Figure 6: Walk induces activity in multiple functional components across the brain at start of walk.

Walk-onset triggered average activity for pan-neuronal data in individual active components at 30 Hz or higher temporal resolution. Note that while most components are activated after walk onset, several components show activity before start of walk. See Table 2 for definition of acronyms. N=30 flies, see table in methods for details.

Figure 7: Forced and spontaneous walk elicit highly similar global brain activity.

(**a**) Z-stacks of map of brain regions activated by walk in flies expressing cytosolic GCaMP (pan-Gal4;UAS-GCaMP6m) or synaptically tagged GCaMP (pan-Gal4;UAS-GCaMP6m) (**b**) Time series of active components during spontaneous walk or rest (magenta vs. green). (**c**) Time series of active components during forced walk or forced rest (magenta vs. green). (**d**) R^2 for behavior regression at different conditions (all regions were pooled, spontaneous, forced, forced with severed connection between VNC and brain) (**e**) Correlation coefficient for walk in different functional components. No significant difference was detected between forced and spontaneous walk. (**f**) R^2 for behavior regression for different active components for forced vs. spontaneous walk. (**g**) R^2 difference between brain region activity during forced turn on the ipsilateral side and forced turn on the contralateral side (orange). Lilac shows the difference for spontaneous turns. N=58 flies for spontaneous walk/turn of different genotypes and N=26 flies for forced walk/turn, see table in methods for details. Box plots show: center line, median; box limits, upper and lower quartiles; whiskers, 1.5x interquartile range; points, outliers.

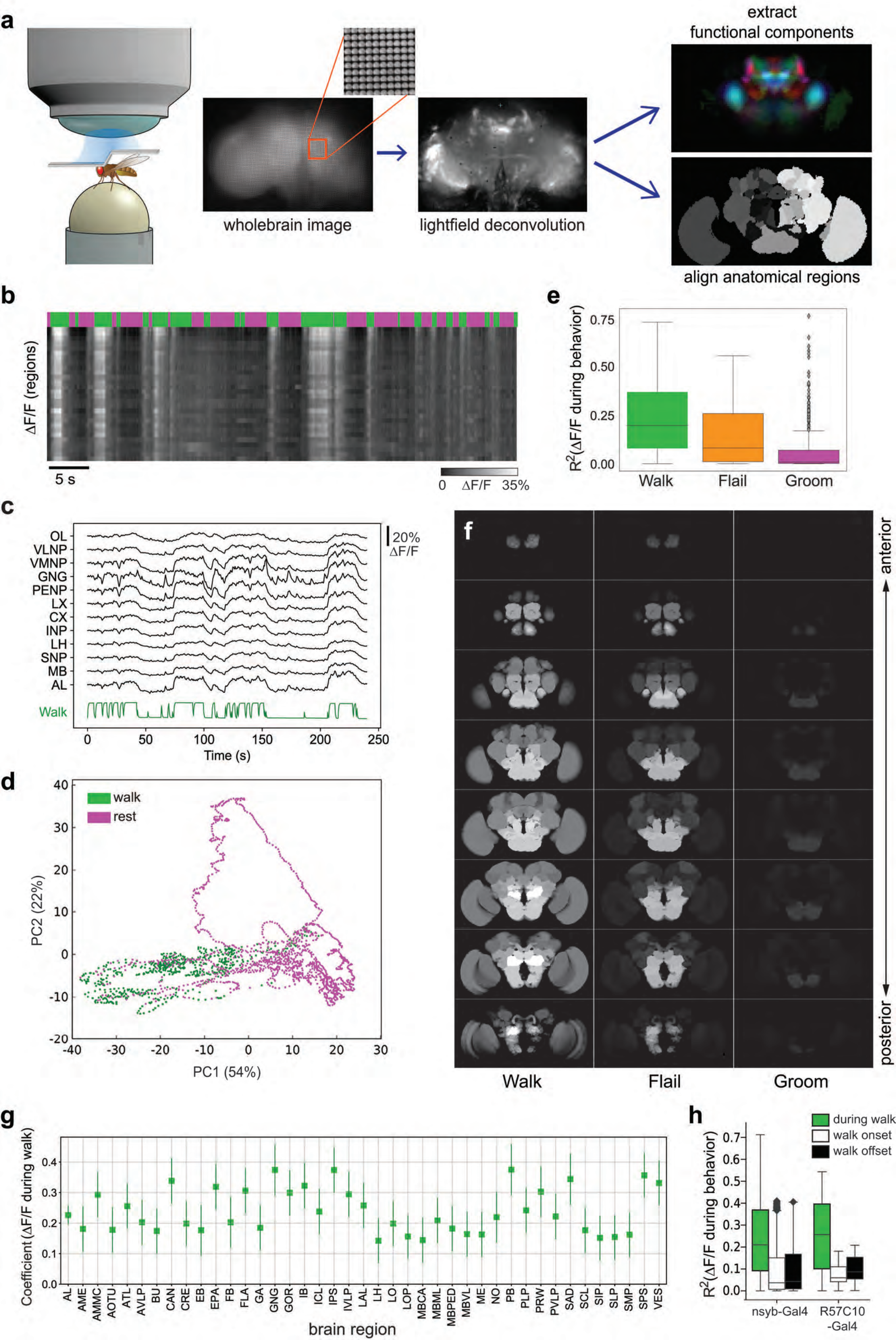
a
wholebrain image
lightfield deconvolution
extract
functional components
align anatomical regions
b
ΔF/F (regions)
5 s
0 ΔF/F 35%
e
R²(ΔF/F during behavior)
0.75
0.50
0.25
0.00
Walk
Flail
Groom
c
OL
VLNP
VMNP
GNG
PENP
LX
CX
INP
LH
SNP
MB
AL
Walk
20% ΔF/F
0
50
100
150
200
250
Time (s)
d
walk
rest
PC2 (22%)
PC1 (54%)
40
30
20
10
0
-10
-20
-40
-30
-20
-10
0
10
20
30
f
anterior
posterior
Walk
Flail
Groom
g
Coefficient (ΔF/F during walk)
0.4
0.3
0.2
0.1
0.0
AL AME AMMC AOTU ATL AVLP BU CAN CRE EB EPA FB FLA GA GNG GOR IB ICL IPS IVLP LAL LH LO LOP MBCA MBML MBPED MBVL ME NO PB PLP PRW PVLP SAD SCL SIP SLP SMP SPS VES
brain region
h
during walk
walk onset
walk offset
R²(ΔF/F during behavior)
0.7
0.6
0.5
0.4
0.3
0.2
0.1
0.0
nsyb-Gal4
R57C10
-Gal4

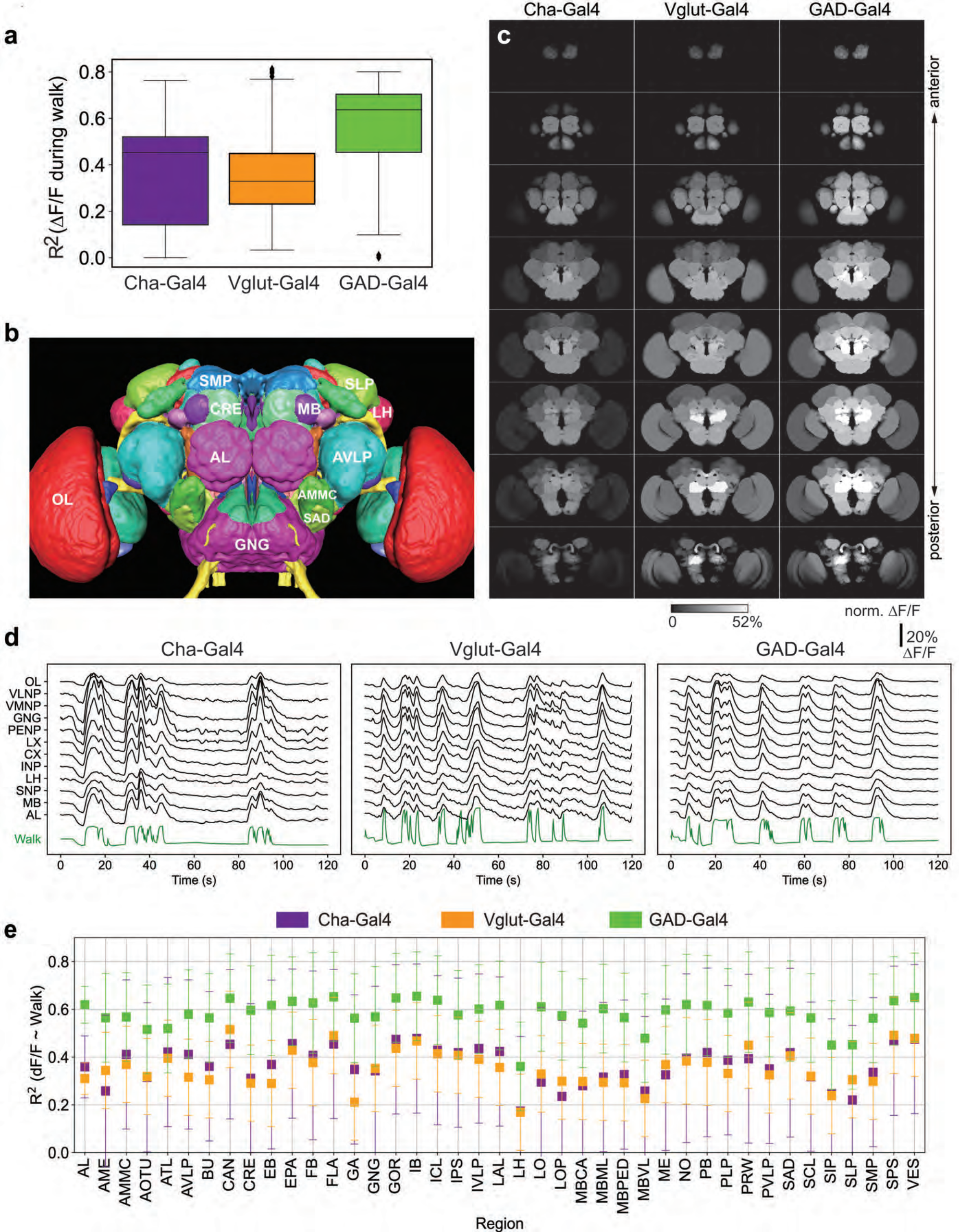
a
R2 (ΔF/F during walk)
0.8
0.6
0.4
0.2
0.0
Cha-Gal4
Vglut-Gal4
GAD-Gal4
b
SMP
SLP
CRE
MB
LH
AL
AVLP
OL
AMMC
SAD
GNG
c
Cha-Gal4
Vglut-Gal4
GAD-Gal4
anterior
posterior
0
52%
norm. ΔF/F
d
Cha-Gal4
Vglut-Gal4
GAD-Gal4
20% ΔF/F
OL
VLNP
VMNP
GNG
PENP
LX
CX
INP
LH
SNP
MB
AL
Walk
0
20
40
60
80
100
120
Time (s)
e
Cha-Gal4
Vglut-Gal4
GAD-Gal4
R2 (dF/F ~ Walk)
0.8
0.6
0.4
0.2
0.0
AL
AME
AMMC
AOTU
ATL
AVLP
BU
CAN
CRE
EB
EPA
FB
FLA
GA
GNG
GOR
IB
ICL
IPS
IVLP
LAL
LH
LO
LOP
MBCA
MBML
MBPED
MBVL
ME
NO
PB
PLP
PRW
PVLP
SAD
SCL
SIP
SLP
SMP
SPS
VES
Region

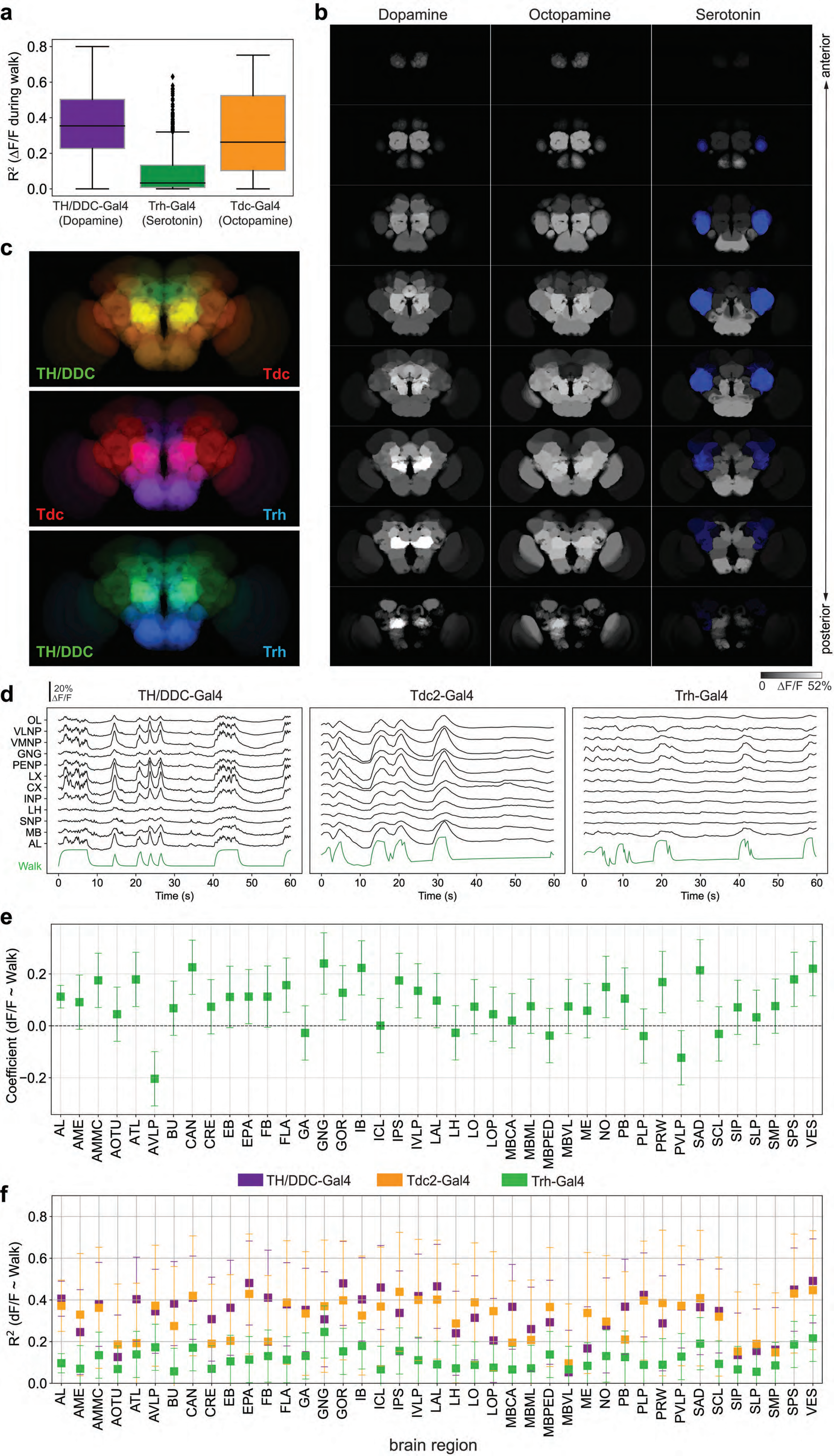
a
R² (ΔF/F during walk)
0.8
0.6
0.4
0.2
0.0
TH/DDC-Gal4 (Dopamine)
Trh-Gal4 (Serotonin)
Tdc-Gal4 (Octopamine)
b
Dopamine
Octopamine
Serotonin
anterior
posterior
0 ΔF/F 52%
c
TH/DDC
Tdc
Tdc
Trh
TH/DDC
Trh
d
20% ΔF/F
TH/DDC-Gal4
Tdc2-Gal4
Trh-Gal4
OL
VLNP
VMNP
GNG
PENP
LX
CX
INP
LH
SNP
MB
AL
Walk
0 10 20 30 40 50 60
Time (s)
e
Coefficient (dF/F ~ Walk)
0.2
0.0
−0.2
AL AME AMMC AOTU ATL AVLP BU CAN CRE EB EPA FB FLA GA GNG GOR IB ICL IPS IVLP LAL LH LO LOP MBCA MBML MBPED MBVL ME NO PB PLP PRW PVLP SAD SCL SIP SLP SMP SPS VES
TH/DDC-Gal4
Tdc2-Gal4
Trh-Gal4
f
R² (dF/F ~ Walk)
0.8
0.6
0.4
0.2
0.0
brain region

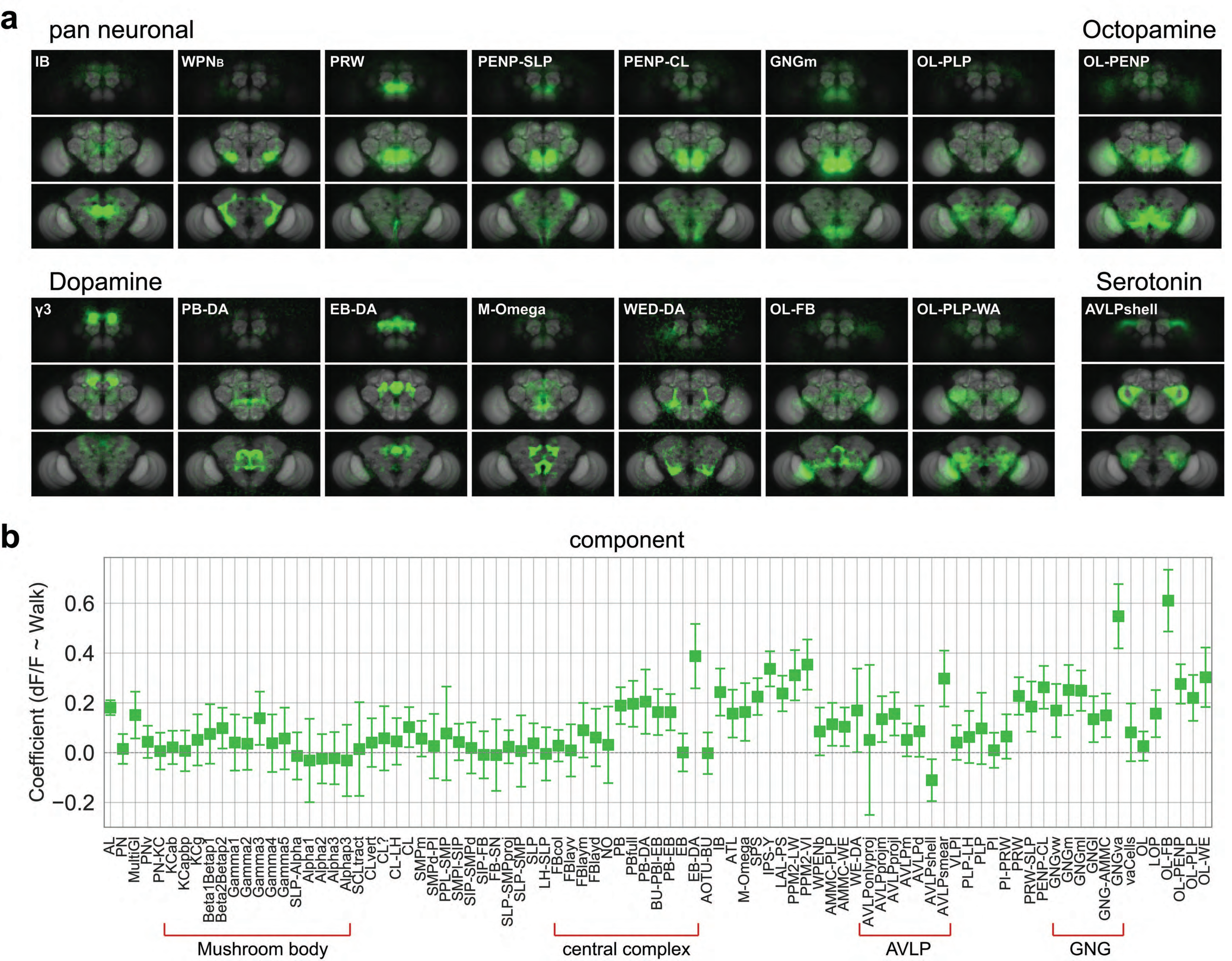
a
pan neuronal
IB
WPNB
PRW
PENP-SLP
PENP-CL
GNGm
OL-PLP
Octopamine
OL-PENP
Dopamine
γ3
PB-DA
EB-DA
M-Omega
WED-DA
OL-FB
OL-PLP-WA
Serotonin
AVLPshell
b
component
Coefficient (dF/F ~ Walk)
0.6
0.4
0.2
0.0
−0.2
AL
PN
MultiGl
PNv
PN-KC
KCab
KCapbp
KCg
Beta1Betap1
Beta2Betap2
Gamma1
Gamma2
Gamma3
Gamma4
Gamma5
SLP-Alpha
Alpha1
Alpha2
Alpha3
Alphap3
SCLtract
CLvert
CL?
CL-LH
CL
SMPm
SMPd-PI
PPL-SMP
SMPI-SIP
SIP-SMPd
SIP-FB
FB-SN
SLP-SMPproj
SLP-SMP
SLP
LH-SLP
FBcol
FBlayv
FBlaym
FBlayd
NO
PB
PBfull
PB-DA
BU-PBI-EB
PB-EB
EB
EB-DA
AOTU-BU
IB
ATL
M-Omega
SPS
IPS-Y
LAL-PS
PPM2-LW
PPM2-VI
WPENb
AMMC-PLP
AMMC-WE
WE-DA
AVLPonlyproj
AVLPprojm
AVLPproj
AVLPm
AVLPd
AVLPshell
AVLPsmear
VLPl
PLP-LH
PLP
PI
PI-PRW
PRW
PRW-SLP
PENP-CL
GNGvw
GNGm
GNGml
GNGl
GNG-AMMC
GNGva
vaCells
OL
LOP
L
OL-FB
OL-PENP
OL-PLP
OL-WE
Mushroom body
central complex
AVLP
GNG

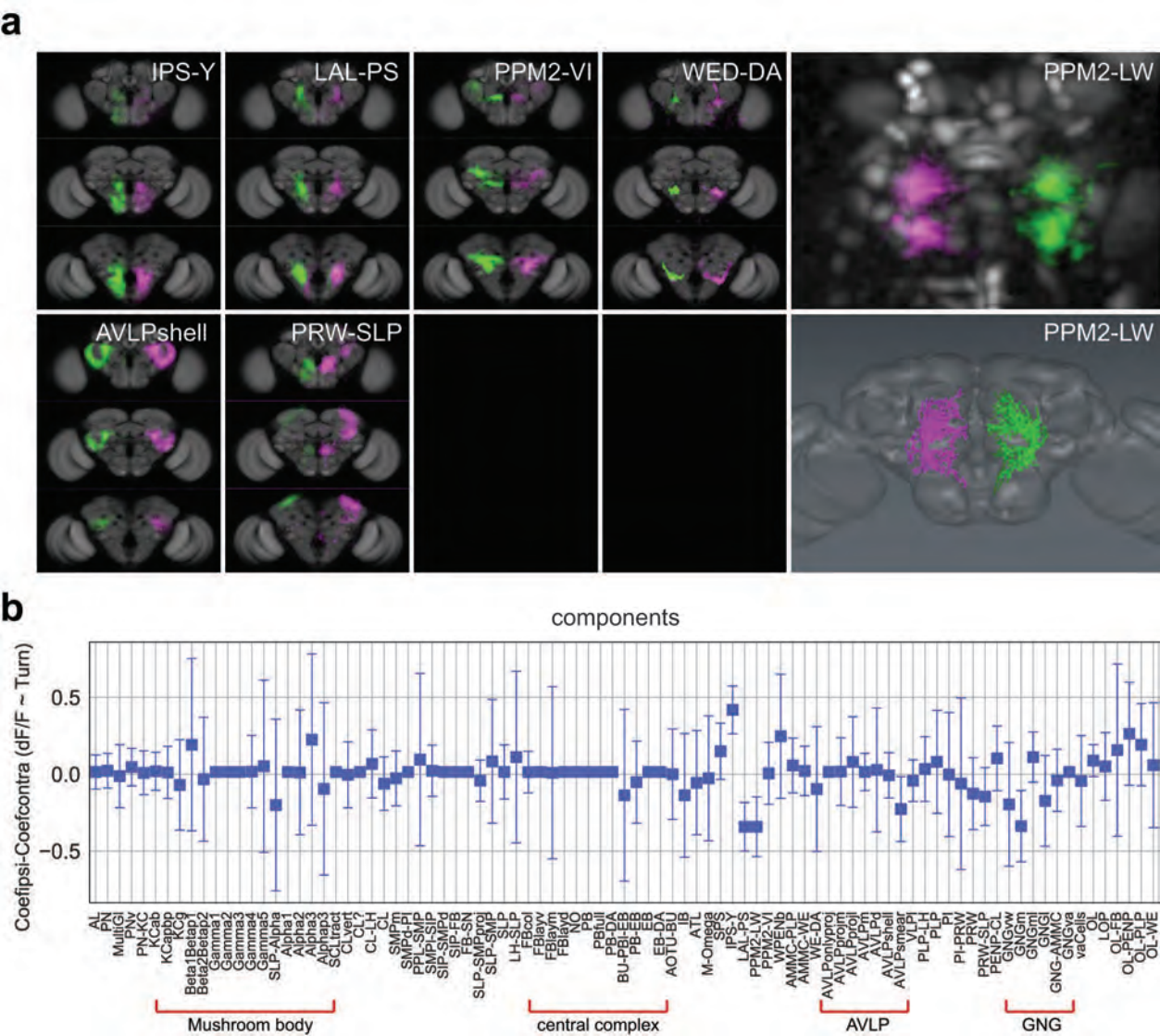
a
IPS-Y
LAL-PS
PPM2-VI
WED-DA
PPM2-LW
AVLPshell
PRW-SLP
PPM2-LW
b
components
Coefipsi-Coefcontra (dF/F ~ Turn)
0.5
0.0
−0.5
Mushroom body
central complex
AVLP
GNG

olfactory system
AL
$n_c = 26$ $n_t = 69$
PN
$n_c = 64$ $n_t = 79$
MultiGl
$n_c = 4$ $n_t = 22$
PNv
$n_c = 37$ $n_t = 78$
mushroom body
β2β'2
$n_c = 15$ $n_t = 79$
γ1
$n_c = 8$ $n_t = 56$
γ2
$n_c = 7$ $n_t = 56$
γ3
$n_c = 4$ $n_t = 18$
γ4
$n_c = 6$ $n_t = 26$
mushroom body
α2
$n_c = 6$ $n_t = 48$
α3
$n_c = 7$ $n_t = 53$
KC-αβ
$n_c = 43$ $n_t = 89$
KC-α'β'
$n_c = 13$ $n_t = 63$
KC-γ
$n_c = 10$ $n_t = 50$
CL?
$n_c = 8$ $n_t = 51$
superior proto-cerebrum
SMPl-SIP
$n_c = 21$ $n_t = 85$
SIP-FB
$n_c = 6$ $n_t = 21$
SLP
$n_c = 11$ $n_t = 58$
LH-SLP
$n_c = 6$ $n_t = 38$
SLP-SMPproj
$n_c = 67$ $n_t = 110$
SMPm
$n_c = 11$ $n_t = 78$
central complex
FBlaym
$n_c = 8$ $n_t = 92$
FBlayd
$n_c = 5$ $n_t = 28$
NO
$n_c = 4$ $n_t = 49$
PB-EB
$n_c = 23$ $n_t = 56$
EB
$n_c = 19$ $n_t = 74$
EB-DA
$n_c = 4$ $n_t = 34$
posterior regions
IB
$n_c = 7$ $n_t = 20$
M-Omega
$n_c = 6$ $n_t = 43$
SPS
$n_c = 16$ $n_t = 49$
IPS-Y
$n_c = 25$ $n_t = 85$
LAL-PS
$n_c = 26$ $n_t = 72$
lateral proto-cerebrum
AVLPprojm
$n_c = 7$ $n_t = 27$
AVLPm
$n_c = 31$ $n_t = 108$
AVLPshell
$n_c = 8$ $n_t = 19$
AVLPsmear
$n_c = 4$ $n_t = 18$
VLPl
$n_c = 17$ $n_t = 61$
PLP-LH
$n_c = 4$ $n_t = 7$
ventral regions
PRW
$n_c = 17$ $n_t = 84$
PRW-SLP
$n_c = 7$ $n_t = 51$
PENP-CL
$n_c = 4$ $n_t = 23$
GNGm
$n_c = 5$ $n_t = 43$
GNGml
$n_c = 12$ $n_t = 30$
visual system
OL
$n_c = 47$ $n_t = 66$
OL-FB
$n_c = 4$ $n_t = 26$
OL-PENP
$n_c = 10$ $n_t = 44$
OL-PLP
$n_c = 8$ $n_t = 23$
OL-PLP-WE
$n_c = 7$ $n_t = 41$
AOTU-BU
$n_c = 13$ $n_t = 49$
norm. dF/F
-0.5
0
0.5
t [sec]

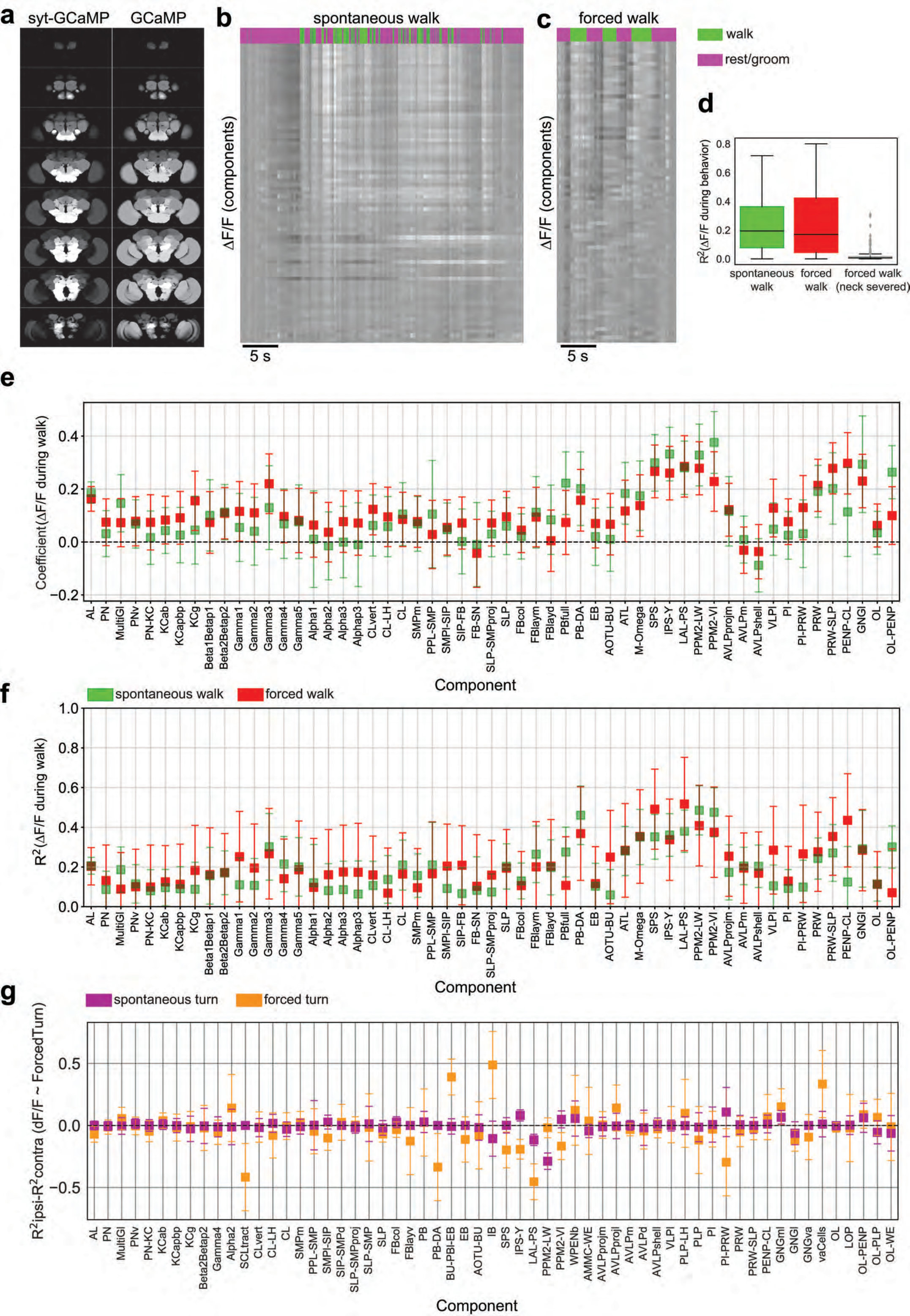
a
syt-GCaMP
GCaMP
b
spontaneous walk
ΔF/F (components)
5 s
c
forced walk
ΔF/F (components)
5 s
walk
rest/groom
d
R²(ΔF/F during behavior)
spontaneous walk
forced walk
forced walk (neck severed)
e
Coefficient(ΔF/F during walk)
Component
f
spontaneous walk
forced walk
R²(ΔF/F during walk)
Component
g
spontaneous turn
forced turn
R²ipsi-R²contra (dF/F ~ ForcedTurn)
Component